Published in final edited form as:
Dev Dyn. 2009 March ; 238(3): 554–571. doi:10.1002/dvdy.21864.

Presynaptic Secretion of Mind-the-Gap Organizes the Synaptic Extracellular Matrix-Integrin Interface and Postsynaptic Environments

Emma Rushton[†], **Jeffrey Rohrbough**[†], and **Kendal Broadie**[*]
Department of Biological Sciences, Vanderbilt Brain Institute, Vanderbilt Kennedy Center for Research on Human Development, Vanderbilt University, Nashville, Tennessee

Abstract

Mind-the-Gap (MTG) is required during synaptogenesis of the *Drosophila* glutamatergic neuromuscular junction (NMJ) to organize the postsynaptic domain. Here, we generate MTG::GFP transgenic animals to demonstrate MTG is synaptically targeted, secreted, and localized to punctate domains in the synaptic extracellular matrix (ECM). *Drosophila* NMJs form specialized ECM carbohydrate domains, with carbohydrate moieties and integrin ECM receptors occupying overlapping territories. Presynaptically secreted MTG recruits and reorganizes secreted carbohydrates, and acts to recruit synaptic integrins and ECM glycans. Transgenic MTG::GFP expression rescues hatching, movement, and synaptogenic defects in embryonic-lethal *mtg* null mutants. Targeted neuronal MTG expression rescues mutant synaptogenesis defects, and increases rescue of adult viability, supporting an essential neuronal function. These results indicate that presynaptically secreted MTG regulates the ECM-integrin interface, and drives an inductive mechanism for the functional differentiation of the postsynaptic domain of glutamatergic synapses. We suggest that MTG pioneers a novel protein family involved in ECM-dependent synaptic differentiation.

Keywords

synaptogenesis; induction; neuromuscular junction; synaptic cleft; transsynaptic; lectin; glutamate receptor; *Drosophila*

INTRODUCTION

The establishment, maintenance, and remodeling of synaptic connections require constant intercellular crosstalk. The synaptic extracellular matrix (ECM) environment shapes and enables cell-cell communication and is crucial for mediating this signaling. A complex array of secreted glycoproteins, proteoglycans, and growth factors comprises the ECM, with a growing list of synapse-specific components. Glycoproteins including synapse-specific collagens, fibronectins, laminins, vitronectins, thrombospondins, tenascins, and their transmembrane integrin receptors provide adhesive and signaling mechanisms supporting synaptic target recognition and synaptogenesis (reviewed by Pavlov et al., 2004). Heparan sulfate proteoglycans (HSPG) and chondroitin sulfate proteoglycans (CSPG) embedded in the

*Correspondence to: Kendal Broadie, PhD, Department of Biological Sciences, Vanderbilt University, VU Station B, Box 351634, Nashville, TN 37235-1634. E-mail: E-mail: kendal.broadie@vanderbilt.edu.
[†]Emma Rushton and Jeffrey Rohrbough contributed equally to this work.

Additional supporting information may be found in the online version of this article.

synaptic ECM, such as agrin, perlecan, and syndecan, bind to signaling factors and cell surface molecules (reviewed by Bernfield et al., 1999; Whitelock and Iozzo, 2005; Van Vactor et al., 2006). Secreted growth factors, including fibroblast growth factor (FGF) and heparin-binding growth-associated molecule (HB-GAM), are regulated by their association with ECM components (reviewed in Pavlov et al., 2004). Thus, the synaptic ECM provides a scaffold supporting the wide range of transsynaptic signaling interactions shaping synapse structure and function.

At vertebrate neuromuscular synapses, presynaptic inductive signals, regulated via the synaptic cleft ECM environment, direct local upregulation of synaptic acetylcholine receptor (AChR) expression and AChR clustering/maintenance within the postsynaptic domain, and downregulation of nonsynaptic AChRs. The presynaptically secreted HSPG agrin signals via the MuSK receptor complex, and its effector Rapsyn, to promote synaptic AChR clustering/maintenance (Gautam et al., 1995, 1996; DeChiara et al., 1996; Lin et al., 2001; Moransard et al., 2003; Misgeld et al., 2005; Kummer et al., 2006). Additional synaptic cleft ECM components, including HB-GAM, laminin, and midkine, and transmembrane integrin receptors, contribute to both agrin-dependent and agrin-independent mechanisms regulating AChR domain assembly (Vogel et al., 1983; Peng et al., 1991, 1995; Daggett et al., 1996; Zhou et al., 1997; Burkin et al., 2000; Marangi et al., 2002; Moransard et al., 2003; Schwander et al., 2004; Weston et al., 2007). Glycan side-chains have been demonstrated to be important in these processes. For example, mutant MuSK protein lacking N-glycosylation sites can be activated by phosphorylation in the absence of agrin (Watty and Burden, 2002). Moreover, both agrin-dependent and independent AChR clustering is modulated by muscle surface GalNAc or α-galactosides (Martin and Sanes, 1995; Park-homovskiy and Martin, 2000). The ECM environment and carbohydrate composition of the ECM is thus critical for transsynaptic signaling regulating postsynaptic assembly.

Carbohydrate-binding lectins have been instrumental for visualizing and defining synaptic ECM. *Dolichos biflorus* agglutinin (DBA) binds a synapse-specific carbohydrate of rat synaptic cleft basal lamina (Sanes and Cheney, 1982; Iglesias et al., 1992). *Vicia villosa* agglutinin (VVA) recognizes mouse/rat NMJ (Scott et al., 1988), and VVA and *Wisteria floribunda* agglutinin (WFA) label chondroitin sulfate components of perineuronal nets in the rat CNS (Hartig et al., 1994; John et al., 2006). Peanut agglutinin (PNA) recognizes cleft ECM at frog NMJ and in flanking perisynaptic Schwann cells (Chen and Ko, 1994; Koirala et al., 2000). Wheat germ agglutinin (WGA) also labels synaptic targets as well as nonsynaptic ECM in a number of species including rat (Ribera et al., 1987; Iglesias et al., 1992). Lectins have been used to study synaptic connectivity, for example in olfactory bulb glomeruli (Saito et al., 1999); in particular, DBA recognizes both pre- and postsynaptic partners during periods of synaptogenesis and remodeling (St John and Key, 2002; Tisay et al., 2002). Integrins represent a key class of glycosylated ECM receptors that are selectively enriched at synapses, including central glutamatergic synapses and NMJs (Cohen et al., 2000; Lin et al., 2003; Shi and Ethell, 2006). Integrins function as αβ dimers, some of which bind arginine-glycine-aspartate (RGD) motifs present in many ECM ligands, and are involved in bidirectional matrix and intracellular signaling pathways (van der Flier and Sonnenberg, 2001; Bokel and Brown, 2002; Hynes, 2002). Integrin interactions with synaptic basal lamina molecules, including laminin and agrin, have roles in neuronally regulated AChR (Burkin et al., 1998) and dystrophin (Rooney et al., 2006) clustering. Integrins at central glutamatergic synapses also have demonstrated roles in synaptogenesis (Chavis and Westbrook, 2001; Shi and Ethell, 2006) and plasticity (Bahr et al., 1997; Staubli et al., 1998; Chan et al., 2003, 2006; Kawaguchi and Hirano, 2006; Kramar et al., 2006).

At the *Drosophila* glutamatergic neuromuscular synapse, presynaptic innervation induces glutamate receptor (GluR) clustering, and thereafter continues to regulate GluR abundance in

the postsynaptic domain (Broadie and Bate, 1993; Featherstone et al., 2000, 2002). Transsynaptic and ECM signaling pathways regulate synapse area, bouton number, presynaptic active zone formation, and postsynaptic GluR clusters. For example, the protein tyrosine phosphatase LAR binds the HSPG syndecan to promote growth of the presynaptic terminal, and the HSPG dallylike to regulate active zone development (Johnson et al., 2006). HSPGs are known to modulate the signaling efficiency of secreted wingless (wg), hedgehog and the bone morphogenetic protein (BMP) decapentaplegic (Bornemann et al., 2004, 2008; reviewed by Hacker et al., 2005). Similar mechanisms likely operate in the BMP glass-bottomed boat/wishful thinking synaptic homoeostasis pathway, and the wg/frizzled pathway coordinating synapse growth and assembly of the postsynaptic GluR domain (Packard et al., 2002; Mathew et al., 2005; Ataman et al., 2008).

As in vertebrates, *Drosophila* ECM-receptor interactions, such as between laminin A and its position-specific (PS) integrin receptor, mediate synaptic adhesion between nerve and muscle (Prokop et al., 1998). We and others have shown previously that synaptic αβPS integrins regulate synaptic architecture (Beumer et al., 1999, 2002), as well as functional synaptic transmission strength (Beumer et al., 1999; Suzuki et al., 2002) and plasticity (Grotewiel et al., 1998; Rohrbough et al., 2000). PS integrin receptors physically associate in a postsynaptic complex with the discs large (DLG) PDZ-domain scaffold, Fasciclin II (FASII) cell adhesion molecule, and CaMKII signaling machinery known to contribute to synaptic GluR assembly and anchoring (Beumer et al., 1999; Albin and Davis, 2004; Chen and Featherstone, 2005; Chen et al., 2005). Dystrophin provides another link between synaptic ECM and postsynaptic signaling/scaffold molecules (van der Plas et al., 2006; Bogdanik et al., 2008). Thus, transsynaptic signals, specifically including ECM-integrin receptor signaling, are known to play key roles in synaptogenesis and synapse modulation at the *Drosophila* neuromuscular synapse.

We previously described *mind-the-gap* (*mtg*), a gene we discovered in a mutant screen for impaired neuromuscular synaptogenesis (Rohrbough et al., 2007). Null *mtg* mutants are 100% embryonic lethal and paralyzed, with severe disruption of postsynaptic GluR domain assembly. Transgenic RNAi studies suggest that neuronal MTG is required to drive postsynaptic differentiation, leading to the hypothesis that MTG is required for an anterograde inductive signaling pathway. The *mtg* candidate gene product is a predicted secreted protein, with sequence homology to glycan-binding proteins and structural homology to signaling families including EGFs (Rohrbough et al., 2007). Here we demonstrate transgenic rescue of these mutant phenotypes to provide conclusive proof of the *mtg* gene identity. Using a MTG::GFP fusion protein, we show that neuronally expressed MTG is specifically targeted to synapses and synaptically secreted in vivo. We show that MTG regulates the extracellular distribution of select lectin-binding glycans, as well as the synaptic localization of PS integrin ECM receptors. Using targeted MTG::GFP expression, we demonstrate that the functional requirement for this MTG regulation originates in the presynaptic cell. These results support the conclusion that MTG is an anterograde inductive signal during synaptogenesis that regulates both the synaptic ECM environment and ECM receptors, and is critical for driving postsynaptic assembly.

RESULTS

Genetic Rescue of *mtg* Null Embryonic Lethal Mutants

Our previously published mapping and cloning of *mtg* indicated that the embryonic lethal mtg^{1} mutation is caused by a single point mutation in the CG7549 gene, resulting in early termination (Rohrbough et al., 2007). Additional *mtg* mutant alleles were created by P-element transposon insertions within, or adjacent to, exon 1 of CG7549. Precise P-element excision resulted in restored viability, and a UAS-RNAi construct against CG7549 partially

phenocopied *mtg* mutant defects, further supporting gene identity (Rohrbough et al., 2007). To conclusively validate *mtg* gene identity, as well as create a tagged MTG protein for incisive assays, we have now generated a CG7549::GFP fusion cDNA downstream of the UAS promoter. A full-length CG7549 cDNA incorporating all the predicted exons was generated using 5′ RACE (see Experimental Procedures section) and cloned into the pUAST vector as a fusion with the eGFP coding sequence. The UAS-CG7549::GFP transgene was then stably integrated in the genome and crossed into the homozygous mtg^1/mtg^1 null mutant background.

Null mtg^1 embryos show a complete absence of coordinated movement and failure to hatch, resulting in 100% lethality of paralyzed mature mutant embryos. Mutant embryos manually removed from the eggcase also display no movement, and have a weakened cuticle typically accompanied by posterior gut herniation. When UAS-CG7549::GFP is driven ubiquitously with UH1-GAL4 in the homozygous mtg^1 null mutant background (mtg^1; UH1:MTG), 50–90% of mtg^1 mutant embryos are rescued to hatch. These rescued larvae display coordinated locomotory movement, and have normal larval appearance/anatomy, including rescue of the cuticle defect. Thus, introduction of the wildtype CG7549 transgene is able to rescue both neurological and non-neural *mtg* null mutant phenotypes. The majority of rescued mtg^1; UH1:MTG animals die in larval stages. This delayed lethality is likely due to failure of UH1-GAL4 to adequately reproduce the normal MTG expression pattern and level during larval life. On average, 50% of mtg^1; UH1:MTG animals that survive to the 3rd instar are fully rescued to adulthood, and overall up to 20% of mtg^1/mtg^1 mutants are completely rescued to adulthood by ubiquitous CG7549::GFP expression. The genotype of rescued animals was confirmed by sequencing.

These results demonstrate that a single copy of the UAS-CG7549::GFP transgene is able to confer rescue to adulthood from complete embryonic mtg^1 lethality. In contrast, ubiquitous CG7549 overexpression is clearly detrimental in wildtype animals. Heterozygote *mtg1*/+ mutant animals ubiquitously expressing a single copy of CG7549 display normal viability. However, wildtype animals overexpressing a single copy of CG7549 display substantial larval lethality and reduced adult viability. Driving transgene expression only in neurons with the neural-specific *elav*-GAL4 driver (mtg^1; elav:MTG) does not rescue viability, consistent with a requirement for *mtg* in non-neuronal as well as neuronal tissues. However, *elav*-GAL4 in combination with UH1-GAL4 increased full adult rescue by >3-fold at 18°C, consistent with a neural requirement for *mtg* gene function. Driving UAS-CG7549::GFP with the reportedly mesodermal GAL4 driver 24B (Brand and Perrimon, 1993) resulted in 18–32% hatching of mtg^1; 24B: MTG embryos in multiple trials; however, all these larvae die within a few minutes of hatching. 24B-GAL4 is an enhancer trap insertion in *held out wings* (*how*) (Fyrberg et al., 1997), and *how* mutants display defects in the epidermis, in embryos (dorsal closure) and adult (wing blisters) (Walsh and Brown, 1998). This suggests that *how* may also be expressed in ectodermal tissues, including neurons. Consistent with this possibility, 24B-GAL4 rescues the mtg^1 cuticle herniation defect.

Taken together, these results conclusively validate *mtg* gene identity as CG7549, and support an essential requirement for MTG function in both neurons and non-neuronal tissue. These results also indicate that normal development and viability is critically dependent on the level and tissue-specificity of *mtg* gene expression. The CG7549::GFP transgene is hereafter referred to as MTG::GFP.

MTG Is Subcellularly Targeted to Synapses

GAL4-UAS control of the transgenic MTG::GFP fusion protein provides a sensitive method to specifically assay subcellular protein trafficking and localization in the nervous system. We examined UH1-GAL4-driven MTG::GFP in transgenically rescued homozygous $mtg1/mtg^1$ null mutants (mtg^1; UH1:MTG), which lack all endogenous MTG protein. In mtg^1; UH1:MTG

mature embryos and newly hatched larvae, MTG::GFP native fluorescence is specifically enriched in the synaptic neuropil (NP) of the ventral nerve cord (VNC) (Supp. Fig. S1, which is available online). Under confocal imaging, both native MTG::GFP fluorescence in semi-dissected animals, and anti-GFP immunostaining in fixed and detergent-permeablized preparations, is clearly localized to punctate aggregates distributed both longitudinally and transversely within the VNC synaptic neuropil (Fig. 1A–D and Supp. Figs. S1, S2). Neuronally-driven MTG::GFP expression in a wildtype mtg^{+} background *(elav*:MTG) was comparable to that in rescued animals (Fig. 1C,D, Supp. Fig. S2, and data not shown). Thus, MTG protein appears selectively targeted to, and concentrated at, neuronal synapses.

To visualize the distribution and extent of synaptic expression, MTG::GFP was examined in nervous system co-labeled for the presynaptic active zone protein bruchpilot (BRP) (Wagh et al., 2006), which defines neurotransmitter release sites as well as clearly revealing the dimensions and boundaries of the synaptic neuropil (Fig. 1A–D). Confocal Z-series and orthogonal projections reveal that MTG puncta are present throughout the VNC synaptic neuropil, but most prominently concentrated in the medial and central regions of the ventral neuropil. In this region, MTG puncta are clearly concentrated along several longitudinal axonal tracts that are completely contained within the BRP-labeled synaptic neuropil (Fig. 1B, D) and that appear to correspond to previously described central intermediate and ventral medial longitudinal tracts (Landgraf et al., 2003). Although little is known of the mapping of different classes of synaptic connections, the neuropil contains excitatory cholinergic synapses between inter- and motor neurons driving locomotory output, in addition to GABAergic and glutamatergic connections (Baines et al., 1999, 2001; Rohrbough and Broadie, 2002; Daniels et al., 2008). Thus, MTG is potentially targeted to multiple central synapse classes, and comparably targeted to the same central synaptic regions regardless of whether MTG::GFP is driven neuronally or ubiquitously. While MTG punctae are entirely surrounded by BRP-defined synaptic punctae, we find that individual MTG::GFP and BRP punctae in thin optical sections are only rarely co-localized exactly (Fig. 1B, D). Rather, MTG punctae typically closely appose BRP punctae, suggesting that MTG predominantly localizes adjacent to presynaptic active zones. The extent and density of MTG::GFP synaptic expression are increased in mature larvae (Fig. 1C,D; see also Supp. Fig. S2A–D), consistent with synaptic elaboration during larval development; however, the general pattern of synaptic expression is established in pre-hatching embryos during synaptogenesis and maintained thereafter.

MTG::GFP aggregates are also detected within neuronal soma (Supp. Fig. S2), including dorsal glutamatergic motor neurons, and within central neuronal processes (Fig. 1C,D). Similar punctate MTG aggregates are observed within the segmental peripheral nerves, both near the nerve exit point from the VNC and in peripheral nerve branches (data not shown), suggesting that MTG is packaged in vesicles and transported along axonal processes. At the large, accessible larval neuromuscular junctions (NMJ), MTG::GFP punctae are clearly localized within presynaptic motor axons near muscle innervation sites and within NMJ presynaptic boutons (Fig. 1E), suggesting that MTG is axonally transported to both central and peripheral synaptic sites. Detailed examination of *elav*-GAL4-driven MTG::GFP fluorescence was made at the NMJ. Under detergent-free conditions to prevent cell permeablization, large type I (Ib; >2-μm diameter) synaptic boutons (Johansen et al., 1989; Atwood et al., 1993; Budnik, 1996; Stewart et al., 1996) typically contain both intense punctate MTG::GFP domains, as well as fainter, diffuse surrounding areas of MTG::GFP (Fig. 1E). Smaller type I (Is; 1–2-μm diameter) and type II (<1-μm diameter) synaptic boutons (Johansen et al., 1989; Atwood et al., 1993; Budnik, 1996; Stewart et al., 1996) also strongly express MTG::GFP. Anti-GFP was used to amplify detection of synaptically localized MTG::GFP protein at NMJ boutons. Anti-GFP and anti-BRP costaining shows numerous MTG punctae in close proximity with BRP-labeled presynaptic active zones (Fig. 1F). As in the central synaptic neuropil, MTG punctae are found closely apposed or adjacent to BRP-labeled active zones, and only infrequently

colocalized directly with BRP punctae (Fig. 1F, right panels). This is consistent with the prediction that MTG is targeted for secretion and packaged in dense-core vesicles, and localizes near but not directly at synaptic release sites. Additionally, UH1-GAL4-driven MTG::GFP also localizes to non-synaptic muscle attachment domains, which accumulate cell adhesion and matrix proteins, including the ECM integrin receptors, PDZ domain scaffold DLG, and dPak kinase (data not shown). These data show that GAL4-driven transgenic MTG is synaptically targeted, and concentrated at both central and peripheral synapses.

MTG Is Secreted to Occupy Punctate Extracellular Synaptic Domains

MTG contains an N-terminus signal peptide and a carbohydrate-binding domain analogous to domains found in extracellular proteins such as growth factors and lectins (Rohrbough et al., 2007). We previously demonstrated that in S2 cells transiently transfected with MTG::GFP, the GFP label is detected on the external surface of the unpermeabilized cells. Based on these findings, we hypothesized that MTG is a secreted protein that interacts with the ECM. To test this secretion hypothesis in vivo, we examined transgenic MTG::GFP animals, first taking advantage of the fact that both *elav*-GAL4 and UH1-GAL4 strongly drive MTG::GFP within the embryonic and larval salivary gland (SG). SG cells are large and specialized for secretion, with a well-characterized pathway of polarized vesicular secretion into a defined extracellular lumen (Beckendorf and Kafatos, 1976; Tojo et al., 1987). MTG::GFP native fluorescence is clearly visible within the SG of living animals (Supp. Fig. S1). Confocal imaging of briefly fixed preparations shows secreted MTG::GFP fluorescence to be strongly concentrated within the extracellular SG lumen (Fig. 2A). In contrast, GAL4-driven eGFP in controls is weakly and diffusely expressed within SG cells, and completely absent from the lumen (Fig. 2A, right).

Interestingly, secreted MTG::GFP remains strongly associated with secretory lumenal surface of SG cells (Fig. 2B,C). Confocal images that capture the plane of the secretory cell surface reveal MTG::GFP in structured, honeycombed patches on the fusion-pocked membrane surface (Fig. 2C), strongly suggesting that the secreted MTG protein is bound to the secretory ECM within specific extracellular domains. This secreted MTG::GFP represents the intact transgenic protein, rather than a cleavage product. First, eGFP expressed alone is not secreted into the extracellular space (Fig. 2A, right). Second, anti-GFP Western blots probing *elav*:MTG, *elav*:eGFP, and *elav*-GAL4 from larval head tissue, including salivary glands, detects no indication of MTG::GFP cleavage (Fig. 2D). The predicted size of secreted GFP-tagged MTG after signal peptide cleavage is ~90 kDa, whereas GFP alone is ~30 kDa. In MTG::GFP transgenic animals only, we find a single major product of ~105 kDa (Fig. 2D); this larger MW is presumably due to post-translational modification of the MTG:GFP protein in SG tissue. These modifications appear to differ from those in the whole embryo, as our previous data show a band of ~120 kDa, as well as larger MW bands, for the wildtype MTG protein extracted from embryos (Rohrbough et al., 2007). The 30-kDa GFP band cannot be detected in either pellet or supernatant fractions from MTG::GFP animals (Fig. 2D). In contrast, larvae expressing eGFP alone contain only the 30-kDa band corresponding to GFP, as expected. These results conclusively show that intact MTG is selectively secreted in vivo and associates closely with the secretory cell membrane with an intriguing extracellular pattern near the cell surface.

We next focused on determining whether MTG is secreted at synaptic terminals. *elav*-GAL4-driven MTG::GFP native fluorescence and anti-GFP immunoreactivity were imaged in parallel at the NMJ synapse using detergent-free conditions; under these conditions, anti-GFP access to the cell interior is prevented, allowing extracellularly localized MTG::GFP to be clearly discriminated (Fig. 2E). Native MTG::GFP fluorescence (green; Fig. 2E) is predominantly concentrated within large type I presynaptic boutons. Extracellular anti-GFP fluorescence (red) is strikingly punctate, and localized in aggregates both immediately adjacent to the bouton

surface, as well as in punctae more peripherally surrounding the bouton (arrows, Fig. 2E). In high-magnification images of single synaptic boutons (Fig. 2E, bottom panels), anti-GFP punctae closely localized to the bouton often appear superimposed or partly colocalized with native MTG::GFP concentrated near the bouton perimeter. These areas of overlying GFP/anti-GFP signal (yellow in merged images, Fig. 2E) represent secreted MTG aggregates closely juxtaposed to regions of concentrated internal MTG. Consistent with this interpretation, external anti-GFP puncta localized at the lateral bouton edges show less overlap with native GFP fluorescence and appear mostly red (Fig. 2E, bottom panels). Native GFP fluorescence is only weakly detectable in the surrounding extracellular space in association with anti-GFP puncta, most likely due to the amplified detection sensitivity conferred by anti-GFP and secondary antibody labeling. These results clearly show that neuronally expressed transgenic MTG is secreted from presynaptic boutons, and thereafter binds synaptic matrix targets to occupy spatially constrained punctate extracellular domains.

Drosophila NMJ Synapses Possess Specialized Extracellular Matrix Environments

MTG contains a carbohydrate-binding CBD2 domain (Rohrbough et al., 2007), predicted to bind secreted glycosylated ECM proteins. The *Drosophila* NMJ synaptic cleft contains a specialized ECM, characterized at the ultrastructural level as a regularly patterned, electron-dense honeycomb structure juxtaposed between the pre-and postsynaptic membranes (Prokop, 1999; Rohrbough et al., 2007). We have hypothesized that the synaptic cleft ECM contains targets for MTG binding. We have also shown previously that *Drosophila* integrin receptors, consisting of an essential βPS subunit encoded by *myospheroid* (*mys*), dimerized with one of three known α partners (αPSI/II/III), are concentrated at NMJ synapses (Beumer et al., 1999; Rohrbough et al., 2000). Using standard detergent-permeablized conditions, we previously showed that α/βPS-integrins are localized predominantly at large type Ib boutons (Beumer et al., 1999, 2002), which are surrounded by an extensive subsynaptic reticulum (SSR) (Johansen et al., 1989; Atwood et al., 1993; Stewart et al., 1996). Synaptic α/βPS integrins are colocalized with postsynaptic proteins such as DLG, with which integrin receptors form a direct complex (Beumer et al., 1999, 2002). We, therefore, wished to chart and define the synaptic ECM-integrin interface as a prelude to testing the predicted role of MTG in regulating this extracellular domain.

Using detergent-free conditions to minimize disruption of the ECM and membrane proteins, anti-βPS staining reveals integrin receptors to be concentrated in a broad synaptic ECM domain completely surrounding pre-synaptic boutons (Figs. 3A,E, 4). Consistent with our previous studies, under these conditions integrins are most prominently expressed at type Ib boutons, and more weakly expressed at the smaller type Is boutons, which have less extensive SSR (Johansen et al., 1989; Atwood et al., 1993; Stewart et al., 1996). Integrins are largely undetectable at type II/III boutons (data not shown). Importantly, βPS integrin synaptic staining is typically concentrated in dense punctate domains that extend well beyond the anti-HRP-labeled presynaptic bouton membrane, showing that an ECM environment extends into and surrounds the SSR domain (Fig. 3A,E; Supp. Fig. S3). We found that detergent-free conditions markedly improve the level and consistency of synaptic anti-βPS labeling, indicating that features of the observed punctate βPS domain patterning are susceptible to disruption by detergent.

We next assayed the synaptic ECM carbohydrate landscape under detergent-free conditions using an assortment of lectins, which are reported to bind different combinations of Glc-NAc, GalNAc, and sialic acid residues (see Introduction section). Vicia villosa agglutinin (VVA) binds terminal N-acetyl galactosaminyl (GalNAc) residues. As with βPS integrins, VVA labels neuronal tissue and weakly labels the muscle surface. At the NMJ, VVA clearly and reliably labels the synaptic ECM surrounding large type Ib synaptic boutons (Fig. 3B), more weakly

labels type Is boutons, and is absent from type II/III boutons. In contrast to βPS integrins, however, VVA synaptic labeling is generally homogeneous and non-punctate, and more spatially restricted to the synaptic ECM domain immediately surrounding boutons (Fig. 3B; Supp. Fig. S3A). Since lectins can bind more than one sugar, and may also bind non-carbohydrate epitopes, we repeated VVA staining in the presence of an inhibiting sugar. Pre-incubating VVA for 1 hr in 0.2M GalNac strongly reduced tissue staining (Supp. Fig. S4A), indicating that VVA binding is predominantly specific to the expected sugar. The VVA-binding domain is, therefore, consistent with a general synaptic matrix target distributed throughout the synaptic ECM. In detergent-treated preparations, the pattern and appearance of VVA labeling is similar, and shows a high degree of overlap with anti-DLG, but the overall VVA staining intensity is decreased (data not shown), again underscoring the improved preservation of ECM domains with detergent-free conditions.

Wheat Germ Agglutinin (WGA) binds sialic acid and N-acetyl glucosaminyl residues (GlcNAc), as well as GlcNAc polymers. The MTG CBD domain is predicted to bind the same substrates as WGA, so we were particularly interested in the possibility that WGA and MTG bind to the same in vivo target(s). Under detergent-free conditions, WGA strongly labels punctate domains distributed over the muscles, with WGA-labeled punctae particularly concentrated in the NMJ synaptic ECM domain (Fig. 3C), densely concentrated around the periphery of synaptic boutons. In confocal Z-series projections, WGA-labeled punctae are comparatively absent from the SSR regions directly underlying synaptic boutons; note the near-complete absence of overlap between WGA punctae and HRP (Fig. 3C). However, we observe that WGA diffusely labels this synaptic domain at a much lower level. The prominent WGA-labeled ECM punctae again resemble similar domains concentrating secreted MTG (Fig. 2E) and transmembrane βPS receptors (Fig. 3A). Pre-incubating WGA for 1 hr in 0.2M GlcNAc nearly eliminated tissue staining (Supp. Fig. S4B), indicating that most, if not all, WGA labeling is specific for the expected sugar. Detergent treatment markedly alters the WGA labeling pattern. Although WGA synaptic labeling persists, WGA fluorescence is more tightly and smoothly confined to the outline of the HRP-stained presynaptic membrane, while the prominent, punctate synaptic domains are largely absent (data not shown). We, therefore, find that WGA reveals a synaptic ECM domain at *Drosophila* synapses, similar to reports from vertebrate synapses (Martin, 2003). While WGA and VVA define synaptically-enriched ECM components, other lectin probes define ECM carbohydrates that are specifically excluded from the synaptic domain. Dolichos biflorus agglutinin (DBA) is a reported GalNAc-binding, synapse-specific marker in vertebrate synapses (Martin, 2003). In *Drosophila*, DBA strongly labels segmental nerves and motor axons proximal to the NMJ arbor, but the labeling abruptly decreases and shows virtually no enrichment in NMJ synaptic domains (Fig. 3D). Note that although the binding specificities of DBA and VVA are reportedly similar, their labeling patterns differ completely. This is most likely because the VVA lectin used here (subtype B4) primarily binds terminal GalNAc residues, while binding of the DBA lectin requires trisaccharide-linked GalNAc (EY Laboratories Inc, Catalog and personal communication) (Etzler and Kabat, 1970;Puri et al., 1992). Peanut Agglutinin (PNA) binds to Gal β-1,3 GalNAc-Thr/Ser, and is a well-established synapse-specific ECM marker at the frog NMJ (Martin, 2003). PNA shows no appreciable labeling of *Drosophila* NMJ synapses, and generally provides the weakest signal of the lectins assayed (data not shown). Thus, of the lectins surveyed, only WGA and VVA label synaptic ECM components that are potential targets for regulation by MTG. We note that while secreted MTG, βPS integrin, and VVA- and WGA-lectin binding domains exhibit differences in pattern and distribution, they also appear to occupy largely overlapping synaptic domains (Supp. Fig. S3A). To directly address whether the secreted, extracellular MTG::GFP ECM domains described above (Fig. 2E) overlap with βPS ECM domains, we co-labeled NMJs in elav:MTG::GFP larvae for βPS and MTG::GFP under detergent-free conditions, using anti-GFP to detect secreted MTG::GFP. As shown in Figure 3E,F (see also Supp. Fig. S3B), the majority of extracellular MTG punctae

lie directly within the βPS domain, and usually colocalize directly with βPS. Thus, secreted MTG and transmembrane integrin ECM receptors coexist and may interact within specialized extracellular subdomains. Consistent with this finding, the VVA-labeled ECM domain similarly overlaps with or contains secreted extracellular MTG domains (Supp. Fig. S3C).

MTG Is Required for Synaptic Integrin ECM Receptor Localization

If integrin ECM receptors act downstream of MTG function, one prediction is that integrin synaptic localization may be dependent on MTG function. MTG lacks RGD domains, so cannot act as an RGD-containing integrin ligand. However, since secreted extracellular MTG domains overlap with integrin receptor domains at the NMJ synapse, and since MTG is required for formation of the specialized synaptic cleft ECM believed to localize integrin ligands (Rohrbough et al., 2007), MTG could regulate the trafficking and/or maintenance of integrin receptors at the synaptic interface. To test this hypothesis, we examined βPS integrin expression at larval NMJ synapses following presynaptically targeted RNAi-mediated MTG knockdown using the neuronal-specific *elav*-GAL4 driver (*elav:mtg* RNAi).

Presynaptic MTG knockdown (*mtg* KD) strongly decreases the level of βPS integrin synaptic localization at the NMJ, compared with *elav*-GAL4 controls (Fig. 4). However, the severity of βPS loss at the synapse was somewhat variable in different *elav: mtg* RNAi animals and at individual NMJs (Fig. 4A–C), as expected for a partial loss-of-function RNAi condition. Synaptic anti-βPS fluorescence intensity was, therefore, quantified at numerous NMJs, including muscles 6/7, 13, and 4, in multiple paired control and mutant preparations. Mean anti-βPS staining fluorescence at *mtg* KD NMJs was significantly reduced to 70.0% ± 5.0 of control levels (mean ± SEM; $P < 0.002$, Wilcoxon signed rank test; n = 19), demonstrating that presynaptic MTG is required for normal synaptic βPS localization. As a further control, we compared the severity of MTG-dependent βPS reduction to direct genetic removal of βPS, using the strongest available viable transheterozygote combination of the βPS null (mys^{xg43}) and the temperature-sensitive mys^{ts1} allele. The mys^{xg43}/mys^{ts1} animals raised at 29°C are viable to late larval/pupal stages, but mutant βPS integrin expression level is severely reduced at the NMJ (17.8 ± 4.7% of wildtype controls raised at 29°C) and in nonsynaptic muscle (32.7 ± 9.5% of wildtype) (Fig. 4D; Supp. Fig. S5). We have previously shown that this *mys* allelic combination allele displays marked synaptic architecture defects (Beumer et al., 1999), underscoring the importance of βPS integrin in synaptogenesis. These results support the model that presynaptically secreted MTG transsynaptically regulates postsynaptic integrin localization.

MTG Regulates Carbohydrate Environments and Distribution

To assay the role of MTG in regulating the carbohydrate environment, we first utilized the salivary gland (SG) as a well-defined secretion system. In *elav*: MTG transgenic animals, MTG::GFP is prominently localized to cytoplasmic aggregates, including both small (<1 μm) and large (5–15 μm) structures, as well as to a population of 2–5-μm diameter vesicles that are presumably secretory vesicles. Additionally, MTG::GFP is strongly accumulated extracellularly within the SG lumen (Figs. 5A, left; 2A). Thus, MTG::GFP appears along a defined secretory pathway, and is highly concentrated at the secreted endpoint. In control *elav*:eGFP SG expressing eGFP alone, eGFP shows no localized cytoplasmic accumulation or vesicle localization, but rather is concentrated within the nucleus (Fig. 5A, right). In briefly fixed, detergent-treated control SGs, WGA brightly labels nuclear membranes (Fig. 5A, eGFP) and VVA stains the plasma membrane as expected (Fig. 5C, eGFP), but neither lectin co-localizes with eGFP, and strongly lectin-labeled secretory vesicles or cellular aggregates are not observed. In sharp contrast, in SG expressing MTG::GFP, both WGA- and VVA-labeled targets are concentrated to cytoplasmic organelles and secretory vesicles, in a pattern very

similar to MTG::GFP itself (Fig. 5B,D). WGA and VVA also weakly label secreted material in the SG lumen (Supp. Fig. S6).

The colocalization of MTG::GFP and lectin labeling is consistent with their binding to common carbohydrate targets, as predicted. A second possibility is that colocalization is a result of lectins directly binding to glycosylated MTG::GFP. However, while MTG::GFP and lectin labeling strongly overlap in SG cells, GFP and lectin fluorescence intensities are not proportional to each other in colabeled domains, as expected if lectins were to bind MTG directly. For example, WGA-labeled SG vesicles appear similarly colocalized with MTG::GFP and WGA punctae, but in merged images individual punctae often appear more strongly green or red, as well as many that are distinctly yellow (Fig. 5B). Similar results are obtained with VVA labeling. To investigate this further, we carried out experiments in MTG::GFP-expressing SG with Alexa-633-conjugated WGA, to ensure complete spectral separation of GFP and lectin fluors in regions of overlapping expression. As before, although MTG::GFP and WGA exhibit a predicted high degree of colocalization, some areas of strong MTG::GFP signal show weak WGA colabeling, while clearly weaker MTG::GFP accumulations show strong WGA colabeling (Supp. Fig. S6). Similar results are obtained with TRITC-VVA labeling. This lack of proportional labeling suggests that MTG is not a direct target of lectin labeling. We conclude, therefore, that MTG overexpression is able to dramatically redirect the distribution of glycans.

To investigate whether MTG similarly regulates lectin carbohydrate distribution at synapses, and particularly within the synaptic ECM, we assayed WGA and VVA lectin labeling following presynaptically-targeted MTG::GFP over-expression (*elav*:MTG) and pre-synaptic RNAi-mediated MTG knockdown (*elav:mtg* RNAi) (Fig. 6). Experimental *elav*:MTG or *elav:mtg* RNAi and control elaveGFP animals were dissected in pairs, processed and stained in parallel, and imaged identically at the muscle 4 type Ib NMJ (segment A3). As noted above, WGA labels NMJs with two distinctly different patterns: diffuse, low-intensity labeling surrounding the synaptic terminal; and prominent WGA punctae, usually at saturating fluorescence intensity, localized most abundantly at the proximal portion of the NMJ (Fig. 6A). We, therefore, quantified both the average pixel intensity within a defined synaptic region, and the percent-age of the defined region occupied by saturated punctae. Quantified regions for each synapse were created from the dilated outline of the HRP-labeled synaptic terminal, to encompass the surrounding terminal margins (see Experimental Procedures section). The dilated region was then transferred to the WGA-labeled channel for fluorescence measurement. Mean WGA intensity within the defined synaptic regions was significantly increased by 50% at *elav*:MTG NMJs compared to *elav*:eGFP controls (57.6 ± 7.3, control vs. 86.6 ± 7.1, *elav*:MTG; $P = 0.012$, Wilcoxon Signed Rank Test; N = 8 paired NMJs, 4 animals of each genotype) (Fig. 6A). In parallel, the percentage of *elav*:MTG NMJ regions occupied by saturated WGA puncta was significantly increased by ~80% (2.9 ± 1.0%, control vs. 5.2 ± 1.5%, *elav*:MTG; $P = 0.012$) (Fig. 6A). In contrast, the *elav: mtg* RNAi animals failed to show a consistent change in mean WGA labeling intensities ($P = 0.2$, N = 8 paired NMJs, 4 animals of each genotype; data not shown). Synaptic VVA labeling was also quantified within the HRP-labeled NMJ synaptic region. As with WGA, the mean VVA synaptic intensity was significantly increased at *elav*:MTG NMJs compared to controls (61.6 ± 5.2, control vs. 67.2 ± 5.2, elav:MTG; $P = 0.05$, Wilcoxon signed-rank test; N = 11 paired NMJs) (Fig. 6B). We found no significant change in mean VVA labeling intensities in elav:*mtg* RNAi animals (59.9 ± 6.1, control vs. 59.8 ± 5.3, elav:*mtg* RNAi Wilcoxon signed-rank test; N = 14 paired NMJs, 8 animals of each genotype; data not shown). One explanation for this negative result is that lectins bind a range of ECM molecules, of which only a subset are regulated by MTG. In the MTG RNAi partial knockdown condition, a decrease in a subset of ECM glycans may be undetectable. We conclude that presynaptic MTG expression is able to drive the recruitment

of lectin-labeled GlcNAc, sialic acid, and/or GalNAc-bearing glycoproteins to the synaptic ECM domain, but that reduction of MTG does not detectably alter this domain.

Integrins are involved in bidirectional signaling and matrix patterning interactions in many contexts (Hynes, 2002). This raises the intriguing possibility that synaptic integrin receptors may have a role in the establishment and organization of the synaptic cleft carbohydrate matrix. To test this hypothesis, we examined synaptic VVA labeling in mys^{xg43}/mys^{ts1} βPS integrin mutants raised at 29°C, which have >80% loss of synaptic βPS integrin receptors (Fig. 4D and Supp. Fig. S5). Mean VVA synaptic fluorescence at *mys* mutant NMJs is not significantly altered compared to wildtype controls raised at 29°C (Fig. 6C). In contrast, VVA levels in mutant nonsynaptic muscle regions are abnormally elevated (Fig. 6C, right). Quantification of VVA fluorescence both at the NMJ and in nonsynaptic domains in paired control and *mys* mutant preparations confirmed that nonsynaptic VVA level is significantly elevated in *mys* mutants (124.8 ± 8.4% of control; $P = 0.002$; Wilcoxon signed rank test; N = 12). This change is also correlated with a significantly reduced ratio of synaptic: nonsynaptic fluorescence intensity (1.58 ± 0.06, *mys* vs. 1.77 ± 0.08, control; $P = 0.014$, Wilcoxon signed rank test; N = 12; Fig. 6C). Thus, in the absence of synaptic βPS integrin receptors, there is a reduced VVA selectivity for the NMJ synaptic domain, suggesting that synaptic integrins play a role in regulating the synapse-specificity of the specialized ECM domain.

Transgenic MTG Expression Rescues Postsynaptic Assembly in *mtg* Null Mutants

Embryonic lethal *mtg* null mutants exhibit a disrupted postsynaptic density (PSD) domain, including reduced/mislocalized dPix, dPak, DLG, and Dock proteins required for glutamate receptor (GluR) localization (Parnas et al., 2001; Albin and Davis, 2004; Rohrbough et al., 2007). To test whether transgenic MTG::GFP expression rescues these postsynaptic defects, we examined GluR, DLG, and dPak synaptic localization in hatching-stage mtg^1; UH1:MTG embryos. PSD immunostaining was compared to homozygous mtg^1 mutants and wild-type controls (mtg^+), each containing a copy of the UAS-*MTG::GFP* transgene without the UH1-GAL4 driver. UAS-*MTG::GFP*-containing mtg^1 embryos appeared phenotypically identical to genetic mtg^1 null mutants, including 100% hatching failure, complete paralysis, and weak cuticle/gut herniation when manually removed from the eggcase. In sharp contrast, mtg^1; UH1: MTG animals selected at hatching exhibit patterned locomotory movement, normal anatomy, and cuticle integrity, demonstrating functional rescue.

We first examined the synaptic localization of the essential GluRIIC subunit, present in all GluRs (Qin et al., 2005). Synapses were costained for the active zone marker BRP. Control synapses show tight juxtaposition of the presynaptic BRP active zone punctae (red) and the postsynaptic GluR punctae (green; Fig. 7A, left). Null mtg^1 mutant NMJs display exhibit normal, well-differentiated presynaptic BRP labeling comparable to control NMJs, but GluR synaptic punctae are severely reduced both in number and intensity (Fig. 7A, middle). In contrast, mtg^1; UH1:MTG NMJs exhibit markedly improved incidence of colocalized BRP and GluR synaptic puncta, providing strong evidence of rescue of postsynaptic GluR domains (Fig. 7A, right). We next examined postsynaptic DLG and dPak. Wild-type, and control synapses show large DLG synaptic domains (red) and smaller synaptic dPak punctae (green; Fig. 7B, left). Null mtg^1 mutant NMJs show consistently reduced levels of synaptically localized DLG (Fig. 7B, middle). In contrast, at mtg^1; UH1: MTG NMJs, DLG is restored to levels comparable to or even greater than controls (Fig. 7B, right). Similarly, mtg^1 mutants exhibit severely reduced numbers and intensity of dPak synaptic puncta (Fig. 7B, middle), but mtg^1; UH1:MTG NMJs exhibit dPak synaptic enrichment and discrete synaptic punctae (Fig. 7B, right). Thus, transgenic expression of MTG results in clearly evident rescue of DLG and dPak synaptic colocalization (Fig. 7B). These results confirm the requirement of MTG in postsynaptic assembly.

As noted above, when combined with UH1-GAL4-driven MTG, neuronally targeted MTG expression improves the rescue of adult viability. To address whether presynaptic MTG confers rescue of postsynaptic differentiation, we next examined PSD differentiation phenotypes in null *mtg* mutants expressing *elav*-GAL4-driven MTG::GFP (*mtg*^{1}; *elav*:MTG). Embryonic *mtg*^{1}; *elav*:MTG NMJs display normal-appearing presynaptic BRP labeling, indicating normally differentiated presynaptic release sites (data not shown). Importantly, targeted presynaptic expression of MTG in *mtg*^{1}; *elav*:MTG restored punctate dPak synaptic localization and staining intensity (Fig. 7C). In addition, presynaptic MTG consistently rescued synaptic DLG localization compared to *mtg*^{1} null synapses. DLG synaptic levels were in some cases markedly stronger in *mtg*^{1}; *elav*:MTG rescue animals than in *mtg*$^{+}$ controls (Fig. 7C). These results indicate significant rescue of postsynaptic assembly defects by targeted presynaptic expression of MTG::GFP. Thus, transgenic MTG rescue restores normal postsynaptic differentiation in null mutants, supporting the hypothesis that neuronally expressed and locally secreted MTG is required to regulate the developing synaptic ECM-integrin interface and induce postsynaptic differentiation.

DISCUSSION

We have hypothesized that presynaptically secreted Mind-the-Gap (MTG) binds within the synaptic cleft extra-cellular matrix (ECM) to establish the synaptic cleft environment required for inductive signaling pathways driving postsynaptic assembly, including glutamate receptor (GluR) localization/maintenance. We showed previously that the MTG protein contains a predicted secretion signal peptide, and a 6-cysteine domain related to “cysteine-knot” domains, with high homology to the carbohydrate-binding domain (CBD) in ECM-binding protein families (Rohrbough et al., 2007). Endogenous MTG expression peaks sharply during late embryonic stages (16 – 8 hr), corresponding to the period of functional synapse differentiation. The key features of the *mtg* null mutant phenotype include loss of the electron-dense ECM material characterizing the synaptic cleft, a matrix of unknown composition and function; and the reduction/mislocalization of multiple postsynaptic density (PSD) proteins, including dPix, dPak, DLG, and Dock/Dreadlocks, which function in the pathway(s) regulating GluR localization and abundance (Rohrbough et al., 2007). Loss of MTG prevents GluR accumulation at the synapse, resulting in a severe (~80%) loss of the functional postsynaptic glutamate response. Neuronally-targeted *mtg* RNAi knockdown partially phenocopies these defects, supporting the hypothesis of an inductive, presynaptic requirement for MTG in postsynaptic assembly.

Several key questions that were not adequately answered in our earlier studies have been thoroughly addressed here. We conclusively confirm *mtg* gene identity by demonstrating rescue of *mtg* null mutant viability with a single copy of a CG7549 cDNA GFP fusion construct. We further show that *mtg* overexpression is deleterious, demonstrating the need for precise regulation of MTG function, consistent with the sharp temporal regulation of endogenous *mtg* developmental expression levels (Rohrbough et al., 2007). In *mtg* null animals, we first show that the MTG::GFP transgene rescues MTG function. We then show that neuronally expressed MTG is subcellularly trafficked to synapses both in the CNS and at the NMJ. Cell-specific targeting of the MTG::GFP transgene using the GAL4-UAS approach was critical for demonstrating specific neuronal requirements, including presynaptic targeting and secretion of MTG, as well as non-neuronal requirements.

The embryonic and larval central synaptic neuropil contains multiple classes of chemical synapses, including predominantly excitatory cholinergic connections driving glutamatergic motor output, as well as GABAergic and glutamatergic connections and neurosecretory terminals (Rohrbough and Broadie, 2002; Landgraf et al., 2003; Daniels et al., 2008). The entire neuropil contains concentrated synaptic connections, as evident from the dense

presentation of presynaptic active-zone proteins (BRP), synaptic vesicle-associated proteins and vesicular neurotransmitter transporters, and postsynaptic proteins (e.g., DLG) (Landgraf et al., 2003; Daniels et al., 2008) (J.R. and K.B., unpublished data). MTG::GFP is prominently localized in similar punctae distributed primarily along longitudinal axon tracts in central and medial regions of the ventral neuropil. When viewed in thin transverse or longitudinal neuropil sections, most MTG punctae appear closely adjacent to or surrounded by BRP punctae, rather than obviously co-localized with BRP. This finding is consistent with MTG functional synaptic localization both presynaptically near active zones and in secreted extracellular aggregates closely opposed to presynaptic boutons. Since MTG is targeted to and secreted at glutamatergic NMJ terminals, an attractive possibility is that MTG also has a specific parallel function at central glutamatergic synapses. A recent study suggested glutamatergic central synapses are primarily concentrated in dorsal neuropil regions in the larval ventral nerve cord (Daniels et al., 2008). Future localization studies, in combination with glutamatergic- and cholinergic-specific synaptic markers, are needed to identify whether MTG is localized to a particular subclass of chemical synapse.

Utilizing the salivary gland (SG) as an accessible, specialized secretory tissue, we show that transgenically expressed MTG is prominently targeted to SG vesicles, subsequently secreted, and strongly accumulated in the lumen, providing in vivo demonstration of predicted MTG secretory function and validating earlier in vitro studies (Rohrbough et al., 2007). Secreted MTG remains closely associated with the external secretory cell membrane, revealing the profiles of fused vesicles, suggesting that the secreted protein remains bound to ECM. Neuronally expressed MTG::GFP is prominently contained within punctate aggregates both in the central neuropil and at NMJ synaptic boutons. Using detergent-free conditions to directly test secretion at NMJ synapses, we show that MTG aggregates are extracellularly localized immediately surrounding presynaptic boutons. The source of targeted MTG::GFP is entirely presynaptic, showing this externally localized MTG to be secreted from presynaptic terminals.

Our results indicate that secreted MTG occupies subregions of synaptic ECM. Using detergent-free lectin-labeling and immunostaining assays to isolate the extracellular domain, we show that the *Drosophila* NMJ synaptic ECM represents a specialized carbohydrate- and receptor-containing matrix domain, bearing many similarities, but also differences, compared to the vertebrate cholinergic NMJ. A punctate βPS integrin distribution defines a synaptic ECM subdomain surrounding type I synaptic boutons. ECM glycans, revealed by VVA and WGA lectins, occupy characteristic but overlapping subdomains with integrin receptors broadly surrounding the synaptic terminal. Other lectin probes (e.g., DBA, PNA) show no synaptic localization, underscoring the important fact that the synaptic ECM is defined by the exclusion of certain extracellular components, as well as the inclusion of synapse-specific molecules. Importantly, we show that secreted MTG::GFP aggregates localize within this broader ECM environment, overlapping with βPS integrins and VVA distribution, showing that MTG is positioned to interact with integrins and other ECM molecules. One potential interpretation is that MTG has a signaling function via integrins and/or specific glycans, and that these interactions occur in discrete extracellular synaptic signaling domains.

A critical finding is that presynaptic MTG is necessary for normal synaptic integrin localization. βPS is a required subunit in all *Drosophila* synaptic integrin receptor subclasses (Leptin et al., 1989); thus, the MTG-dependent reduction of βPS predicts a concurrent loss of α-integrin proteins and functional synaptic integrin receptors. The importance of bidirectional integrin-ligand interactions and patterning in other tissues (Schwarzbauer and Sechler, 1999; Hynes, 2002) suggests that synaptic PS integrins may have a major role in shaping synaptic cleft ECM organization and composition. Since secreted MTG occupies a subset of the βPS synaptic domain, another possibility is that MTG regulates an ECM integrin ligand, such as laminin-A (Burkin et al., 1998, 2000), which in turn regulates integrin localization or

maintenance within the synapse. It is difficult to assess the absolute requirement for synaptic integrins in ECM regulation because *Drosophila* βPS null mutants (*myospheroid; mys*) are 100% early embryonic lethal, with severely abnormal muscle patterning and altered NMJ morphological differentiation (Prokop et al., 1998) (J.R. and K.B., unpublished data). A residual (~20% of normal) level of NMJ-localized βPS in mys^{xg43}/mys^{ts1} hypomorphs is sufficient for relatively normal synaptic composition, although mutant NMJ morphology and synaptic function are significantly perturbed (Beumer et al., 1999, 2002). In these same mutants, nonsynaptic VVA labeling is abnormally elevated, showing an altered synapse-specificity in ECM glycans with reduced levels of the βPS synaptic integrin receptors.

A second series of critical findings is that the MTG level regulates the lectin-defined carbohydrate distribution in the salivary gland, and that presynaptically targeted MTG modifies NMJ synaptic carbohydrate ECM domains. MTG::GFP strongly overlaps with VVA and WGA fluorescence within SG cells and at the synapse, suggesting that MTG and lectin probes recognize accumulations of similar carbohydrates. Lectins are not primarily recognizing MTG itself, as MTG::GFP and lectin signals can be spatially separated, and where they tightly overlap, their fluorescence intensities are not proportional. Thus, MTG overexpression results in increased recruitment or accumulation of carbohydrates, even in regions where MTG itself is only weakly localized. It is of particular interest to consider the in vivo synaptic glycoproteins and/or glycolipids that are recognized by VVA and WGA, and modulated by MTG expression level. In the synaptic ECM, candidate targets for VVA and WGA include the integrin receptors, which are glycosylated and have a distribution overlapping that of both lectins. However, synaptic VVA labeling persists in βPS *mys* mutants with greatly reduced synaptic integrin levels, suggesting that integrins do not carry the glycans recognized by VVA. An alternative possibility is that integrin glycans are lectin targets, but in *mys* mutants the ECM is remodeled in such a way as to restore these glycan moieties.

One potential synaptic target of VVA is O-linked glycans on dystroglycan (DG), an important postsynaptic ECM receptor linked to the muscle cytoskeleton (Haines et al., 2007). DG has roles in regulating quantal content and vesicle release probability in the presynaptic bouton, and also in recruiting GluRIIB to the postsynaptic domain (Bogdanik et al., 2008; Wairkar et al., 2008). Glycosylation is important for DG function in *Drosophila* muscle (Wairkar et al., 2008). Haines et al. (2007) recently reported that NMJ VVA staining is increased by DG overexpression, but not by overexpression of DG lacking the extracellular mucin domain. If VVA labeling at the NMJ is primarily recognizing DG, alterations in VVA resulting from changes in MTG or βPS integrin expression may be mediated in part through changes in the synaptic localization or modification of the DG receptor. Alternatively, DG may itself be recruiting VVA targets to the NMJ ECM. These possibilities will be addressed in future studies. We stress that we can make no assumptions about which specific glycoproteins or glycolipids are recognized in vivo by a given lectin. Indeed, we recognize that lectins may bind other glycans at lower affinity than their preferred substrate target. However, the inhibition of WGA and VVA in vivo labeling by preincubation with their preferred sugars strongly suggests that these lectins recognize these same carbohydrates at the synapse. Given the possible range of synaptic lectin targets, it is of great interest that MTG is able to significantly regulate the entire lectin-labeled glycan pool.

Finally, we demonstrate that transgenic MTG expression confers rescue of the GluR, dPak, and DLG punctate postsynaptic domains that are severely disrupted in *mtg* null synapses (Rohrbough et al., 2007). This restoration of postsynaptic differentiation occurs in parallel with the demonstrated central neuropil and NMJ MTG synaptic targeting, localized punctate presynaptic expression, and secreted external localization in the ECM, and with restored mutant movement and viability. Together, these results indicate a synaptic requirement for functional rescue. Evidence for clear postsynaptic rescue with neuronal-specific presynaptic MTG

expression supports this conclusion, and is consistent with our previous and present results showing a specific presynaptic requirement for MTG in PSD/GluR and βPS localization. The mechanism for the MTG inductive requirement in postsynaptic assembly remains unknown. If MTG acts through integrins in this pathway, then null βPS mutants would be predicted to show loss or mislocalization phenotypes for at least a subset of PSD and GluR. We currently lack the ability to rigorously test this hypothesis owing to the essential, pleiotropic requirements for *mys* during embryogenesis. Alternatively, MTG may act through unidentified matrix or postsynaptic signaling proteins, perhaps including the dystroglycan complex. Several important questions remain to be addressed in future work, including determining the in vivo binding target(s) of MTG, which additional matrix proteins may interact with or be regulated by secreted MTG, and whether MTG directly or indirectly governs the composition/function of the specialized synaptic cleft microdomain.

EXPERIMENTAL PROCEDURES

Molecular Techniques

The 5′ exon of the *mind the gap* (*mtg)* gene was identified using 5′-rapid amplification of cDNA ends (RACE). An oligo dT primer and a primer to the 5′ exon were used to make a full-length cDNA, which was cloned into pMT-tauGFP (Bunch et al., 1988) from the *Drosophila* Genomics Resource Center. The longest *mtg* isoform was selected to construct the cDNA; this is the only predicted isoform to contain a secretion signal peptide. The pMT vector was digested with EcoR1 and BamH1 to remove the *tau* gene, and *mtg* cDNA was ligated in to make an inframe GFP fusion. This *mtg::GFP* fusion gene was cut out of pRMHA using EcoR1 and Xba1, cloned into pUAST, and the construct then stably transformed into the *Drosophila* genome by Genetic Services Inc. Multiple independent transgene insertion lines were generated, including MTG::GFP14.1 (w; P{w+=UAS-MTG::GFP14.1}), MTG::GFP14.2 (w; P{w+=UAS-MTG::GFP14.2}), both on the second chromosome and MTG:: GFP9.3 (w; P{w +=UAS-MTG:: GFP9.3}) on the third chromosome.

Drosophila Genetics

All animals were reared on standard agar/yeast/molasses/cornmeal food at 25° or 29°C, as indicated, in temperature-controlled incubators. For embryo/L1 studies, eggs laid on sucrose/apple juice/agar plates were collected from timed laying sessions. For larval studies, animals were reared at low density to the L3 wandering stage. The *mtg* stocks used in this study include the mtg^1 null and UAS-*mtg* RNAi transgenic lines (Rohrbough et al., 2007), and the UAS-*MTG::GFP* transgenic lines described above. The control UAS-eGFP stock (P{w^{+mC}=UAS-EGFP}8, w^{1118}) was from the Bloomington stock center. Ubiquitous expression of transgenic lines was driven by UH1-GAL4 (w; P{GAL4-da.G32}UH1) obtained from the Bloomington stock center (Rohrbough et al., 2004). Targeted neuron specific expression was driven by *elav*-GAL4 (P{$w^{+W.hs}$=GawB}$elav^{C155}$) (Lin and Goodman, 1994; Rohrbough et al., 2004). Mesodermal expression was driven by 24B-GAL4 (*w*; P{$w^{+mW.hs}$=GawB}^{how24B}) (Brand and Perrimon, 1993). GFP balancers were: TM3 Actin-GFP (TM3, P{w^{+mC} = ActGFP}-JMR2, Ser^1), TM3 Kr-GFP (TM3 P{GAL4-Kr.C}DC2, P{UAS-GFP.S65T}-DC10, Sb^1) and FM7 Kr-GFP (FM7c, P{GAL4-Kr.C}DC1, P{UAS-GFP.S65T}-DC5, sn^+), all from the Bloomington stock center. Parental stocks generated for this study were: *elav;*mtg^1 (*w*, *elav*-GAL4; *st*, mtg^1, *cu*/TM3 Actin-GFP), UH1, mtg^1 (*w* ; UH1-GAL4, st, mtg^1, cu/TM3 Kr-GFP), UAS MTG::GFP14.1; mtg^1/TM3 Kr-GFP. Experimental genotypes were: for neuronal OE, elav:MTG (elav/+ or Y; UAS MTG::GFP14.1 or 9.3/+); for ubiquitous rescue of *mtg*, mtg^1; UH1:MTG (UAS MTG::GFP14.1/+; UH1, *mtg1/*mtg^1); for neuronal rescue of *mtg*, mtg^1; *elav*:MTG (*elav*/+; UAS MTG::GFP14.1/+; *mtg1/*mtg^1); for mesodermal rescue of *mtg*, mtg^1; 24B:MTG (UAS MTG::GFP14.1/+; 24B, *mtg1/*mtg^1); for neuronal RNAi, elav;mtgRNAi (elav/Y; mtg^1/UAS-*mt-g*RNAi). The βPS integrin mutants used were: mys^{ts1}/

mys^{ts1} (Beumer et al., 1999; Jannuzi et al., 2004) crossed to *mys*^{XG43}/FM7 Kr-GFP (Bunch et al., 1992) to generate the transheterozygote *mys*^{ts1}/*mys*^{XG43}.

Immunocytochemistry

Staining was done on mature embryos (20–22 hr after fertilization; AF), early L1 larvae shortly after hatching (22–24 hr AF), and L3 wandering larvae (120–124 hr AF), as previously described (Featherstone et al., 2002; Rohrbough et al., 2004). Control and transgenic embryos and staged larvae were selected from agar plates previously set for timed laying periods. Mature embryos were collected, dechorionated in bleach, and washed in dH_2O. Mutant and rescue animals were selected against a Kr-GFP balancer chromosome. In all experiments, control, mutant and transgenic animals were collected in parallel; and always dissected, processed and imaged in parallel on the same cover slips to allow valid comparison of staining features. Staged embryos and larvae were secured to sylgardcoated cover slips using histoacryl veterinary glue, dissected dorsally, and glued flat. The saline composition in mM: 135 NaCl, 5 KCl, 4 $MgCl_2$, 0.2 mM Ca^{2+}, 5 TES, 75 Sucrose, 2 NaOH, pH 7.2. For glutamate receptor staining, 2 mM glutamate was added to the saline. For MTG::GFP imaging and anti-GFP staining, animals were fixed for 5–10 min in 4% paraformaldehyde (PF). For other immunocytochemistry assays, animals were fixed for 15–30 min in 4% PF or Bouin's picric acid fixative (LabChem Inc, Pittsburgh, PA), or for 5 min in ice-cold MeOH (GluR staining). Washes and dilutions were in phosphate buffered saline (PBS; Invitrogen, Carlesbad, CA); detergent (when used) was 0.1% Triton X (TX, Fisher). Preparations were washed and processed in either PBS-TX (PBS + 0.1% TX) or detergent-free PBS, as indicated. For studies of MTG::GFP expression and lectin-binding in UAS transgenic MTG::GFP and RNAi larvae, wandering 3rd instar larvae were pinned out on sylgard and salivary glands were dissected free, and independently pinned to sylgard.

Antibodies—MTG::GFP distribution was analyzed using FITC-conjugated anti-GFP (Abcam 6662; Cambridge, MA) or unconjugated anti-GFP (Abcam 5450). Central neurons, peripheral axons, and presynaptic NMJ terminals were visualized with FITC-, Texas Red-, or Cy5 conjugated anti-HRP (1:100–1:200; from Jackson Laboratories, West Grove, PA). Presynaptic active zones were stained using antinc82 (bruchpilot [BRP]; 1:100; kindly supplied by Hugo Bellen, Baylor College of Medicine, Houston, TX). Postsynaptic protein staining assays utilized the following antibodies: rabbit anti-GluRIIC (1:500; kindly supplied by Aaron DiAntonio, Washington University, St Louis, MO) and rabbit anti-GluRIID (1:500; kindly supplied by Stephan Sigrist, European Neuro-science Institute Göttingen, Germany), rabbit anti-dPak (1:500, kindly supplied by Lawrence Zipursky, University of California, Los Angeles), mouse ant-DLG mAb 4F3 (1:500, *Drosophila* Hybridoma Bank [DSHB], Iowa), mouse anti-βPS mAb CF6G11 (1:100–1:200, DSHB, Iowa). Primary antibody staining was visualized with Alexa-conjugated secondary probes (Molecular Probes; 1:400 to 1:500, 2 hr at RT).

Lectins—TRITC- or Alexa 633-conjugated VVA, WGA, and DBA from EY Laboratories (San Mateo, CA), and Alexa 488-PNA from Invitrogen, were used at 2–5 μg/ml in PBS. Larval NMJs or SGs were fixed for 5–10 min in 4% PF. To examine extracellular carbohydrate binding, dissected preparations were washed in detergent-free PBS. To examine intracellular carbohydrates, 0.1% TX detergent was added to all washes and reagents. Specificity of lectin binding was tested by incubating 2 μg/ml WGA with 0.2M N-Acetyl-D-glucosamine (Sigma) or 5 μg/ml VVA with 0.2M N-Acetyl-D-Galactosamine (Sigma) for 1 hr at RT before adding lectin to larval NMJ preparations. Vectashield or Fluoromount was used as the imaging medium for all fluorescence microscopy. Confocal scanned images of the CNS, neuromusculature, and salivary glands were acquired on a Zeiss 510 confocal microscope, using Zeiss LSM software and either 40× or 63× oil objectives. Confocal sections and Z-series projections were created

and exported using LSM Image Examiner. Control and mutant images were processed in parallel with Adobe Photoshop software.

Western Blot

To confirm the expression of MTG::GFP, protein size was assayed by Western blot. The *elav*-MTG::GFP, *elav*-eGFP, and *elav*-GAL4 alone (no GFP) genotypes were analyzed. For each genotype, 5 larval heads, including salivary glands, were dissected in saline (composition above), immediately frozen in liquid N2, and ground up on ice. Preparations were homogenized in 50 μl lysis buffer (1× PBS (Invitrogen), 2.5 mM EGTA, 1% Igepal, 1× Complete Mini protease cocktail (Roche). Lysate was centrifuged 10 min at 16,000*g*. Supernatant was removed to fresh tube, and pellet was resuspended in 30 μl PBS. Both supernatant and pellet were boiled 10 min with 1 × NuPAGE LDS sample buffer (Invitrogen) and 5% β-mercaptoethanol, then run on a 4–12% Bis-Tris NuPAGE polyacrylamide gel (Invitrogen) in MOPS buffer. Proteins were transferred to a nitrocellulose membrane, probed with anti-GFP (Abcam 5450) followed by IRDye800-conjugated anti-goat (Rockland), and imaged using the Odyssey infrared imaging system (LI-COR).

Quantification and Statistical Methods

Experimental and control animals were processed and imaged in pairs, under identical conditions. Zeiss LSM Z-stacks were projected flat, and a filtered image saved alongside the original projection. Filtered and unfiltered images were opened in Metamorph software. A region representing the NMJ was generated using the anti-HRP filtered (smoothened) image and an intensity threshold function to outline the synaptic region of interest (ROI). The ROI was then transferred to the VVA unfiltered image. For WGA quantification, the ROI was dilated by a constant amount, to include the bright puncta around the NMJ. Average pixel intensity was logged for each image. For WGA, the area of saturated puncta was logged and expressed as a percentage of total dilated NMJ area. Statistics were calculated in Mstat software, using the nonparametric Wilcoxon Signed Rank test (2-sided). This test applied to paired data measurements calculates the probability of difference between the data sets, and is appropriate even when high variability exists between experiments.

Supplementary Material

Refer to Web version on PubMed Central for supplementary material.

Acknowledgements

We are grateful to Hugo Bellen (Baylor University School of Medicine, Houston, TX), Aaron DiAntonio (Washington University School of Medicine, St. Louis, MO), Stephan Sigrist (European Neuroscience Institute, Göttingen, Germany), and Lawrence Zipursky (University of California, Los Angeles, CA) for antibodies used in this study. The authors gratefully acknowledge the Developmental Studies Hybridoma Bank (DSHB, University of Iowa) for monoclonal antibodies and the Bloomington Stock Center (Bloomington, IN) for fly stocks. This work was entirely supported by NIH grant GM54544 to K.B.

References

Albin SD, Davis GW. Coordinating structural and functional synapse development: postsynaptic p21-activated kinase independently specifies glutamate receptor abundance and postsynaptic morphology. J Neurosci 2004;24:6871–6879. [PubMed: 15295021]

Ataman B, Ashley J, Gorczyca M, Ramachandran P, Fouquet W, Sigrist SJ, Budnik V. Rapid activity-dependent modifications in synaptic structure and function require bidirectional Wnt signaling. Neuron 2008;57:705–718. [PubMed: 18341991]

Atwood HL, Govind CK, Wu CF. Differential ultrastructure of synaptic terminals on ventral longitudinal abdominal muscles in Drosophila larvae. J Neurobiol 1993;24:1008–1024. [PubMed: 8409966]

Bahr BA, Staubli U, Xiao P, Chun D, Ji ZX, Esteban ET, Lynch G. Arg-Gly-Asp-Ser-selective adhesion and the stabilization of long-term potentiation: pharmacological studies and the characterization of a candidate matrix receptor. J Neurosci 1997;17:1320–1329. [PubMed: 9006975]

Baines RA, Robinson SG, Fujioka M, Jaynes JB, Bate M. Postsynaptic expression of tetanus toxin light chain blocks synaptogenesis in Drosophila. Curr Biol 1999;9:1267–1270. [PubMed: 10556094]

Baines RA, Uhler JP, Thompson A, Sweeney ST, Bate M. Altered electrical properties in Drosophila neurons developing without synaptic transmission. J Neurosci 2001;21:1523–1531. [PubMed: 11222642]

Beckendorf SK, Kafatos FC. Differentiation in the salivary glands of Drosophila melanogaster: characterization of the glue proteins and their developmental appearance. Cell 1976;9:365–373. [PubMed: 825230]

Bernfield M, Gotte M, Park PW, Reizes O, Fitzgerald ML, Lincecum J, Zako M. Functions of cell surface heparan sulfate proteoglycans. Annu Rev Biochem 1999;68:729–777. [PubMed: 10872465]

Beumer K, Matthies HJ, Bradshaw A, Broadie K. Integrins regulate DLG/FAS2 via a CaM kinase II-dependent pathway to mediate synapse elaboration and stabilization during postembryonic development. Development 2002;129:3381–3391. [PubMed: 12091308]

Beumer KJ, Rohrbough J, Prokop A, Broadie K. A role for PS integrins in morphological growth and synaptic function at the postembryonic neuromuscular junction of Drosophila. Development 1999;126:5833–5846. [PubMed: 10572057]

Bogdanik L, Framery B, Frolich A, Franco B, Mornet D, Bockaert J, Sigrist SJ, Grau Y, Parmentier ML. Muscle dystroglycan organizes the postsynapse and regulates presynaptic neurotransmitter release at the Drosophila neuromuscular junction. PLoS ONE 2008;3:e2084. [PubMed: 18446215]

Bokel C, Brown NH. Integrins in development: moving on, responding to, and sticking to the extracellular matrix. Dev Cell 2002;3:311–321. [PubMed: 12361595]

Bornemann DJ, Duncan JE, Staatz W, Selleck S, Warrior R. Abrogation of heparan sulfate synthesis in Drosophila disrupts the Wingless, Hedgehog and Decapentaplegic signaling pathways. Development 2004;131:1927–1938. [PubMed: 15056609]

Bornemann DJ, Park S, Phin S, Warrior R. A translational block to HSPG synthesis permits BMP signaling in the early Drosophila embryo. Development 2008;135:1039–1047. [PubMed: 18256192]

Brand AH, Perrimon N. Targeted gene expression as a means of altering cell fates and generating dominant phenotypes. Development 1993;118:401–415. [PubMed: 8223268]

Broadie K, Bate M. Activity-dependent development of the neuromuscular synapse during Drosophila embryogenesis. Neuron 1993;11:607–619. [PubMed: 7691105]

Budnik V. Synapse maturation and structural plasticity at Drosophila neuromuscular junctions. Curr Opin Neurobiol 1996;6:858–867. [PubMed: 9000022]

Bunch TA, Grinblat Y, Goldstein LS. Characterization and use of the Drosophila metallothionein promoter in cultured Drosophila melanogaster cells. Nucleic Acids Res 1988;16:1043–1061. [PubMed: 3125519]

Bunch TA, Salatino R, Engelsgjerd MC, Mukai L, West RF, Brower DL. Characterization of mutant alleles of myospheroid, the gene encoding the beta subunit of the Drosophila PS integrins. Genetics 1992;132:519–528. [PubMed: 1427041]

Burkin DJ, Gu M, Hodges BL, Campanelli JT, Kaufman SJ. A functional role for specific spliced variants of the alpha7beta1 integrin in acetylcholine receptor clustering. J Cell Biol 1998;143:1067–1075. [PubMed: 9817762]

Burkin DJ, Kim JE, Gu M, Kaufman SJ. Laminin and alpha7beta1 integrin regulate agrin-induced clustering of acetylcholine receptors. J Cell Sci 2000;113:2877–2886. [PubMed: 10910772]

Chan CS, Weeber EJ, Kurup S, Sweatt JD, Davis RL. Integrin requirement for hippocampal synaptic plasticity and spatial memory. J Neurosci 2003;23:7107–7116. [PubMed: 12904471]

Chan CS, Weeber EJ, Zong L, Fuchs E, Sweatt JD, Davis RL. Beta 1-integrins are required for hippocampal AMPA receptor-dependent synaptic transmission, synaptic plasticity, and working memory. J Neurosci 2006;26:223–232. [PubMed: 16399691]

Chavis P, Westbrook G. Integrins mediate functional pre- and postsynaptic maturation at a hippocampal synapse. Nature 2001;411:317–321. [PubMed: 11357135]

Chen K, Featherstone DE. Discs-large (DLG) is clustered by presynaptic innervation and regulates postsynaptic glutamate receptor subunit composition in Drosophila. BMC Biol 2005;3:1. [PubMed: 15638945]

Chen K, Merino C, Sigrist SJ, Featherstone DE. The 4.1 protein coracle mediates subunit-selective anchoring of Drosophila glutamate receptors to the postsynaptic actin cytoskeleton. J Neurosci 2005;25:6667–6675. [PubMed: 16014728]

Chen L, Ko CP. Extension of synaptic extracellular matrix during nerve terminal sprouting in living frog neuromuscular junctions. J Neurosci 1994;14:796–808. [PubMed: 8301362]

Cohen MW, Hoffstrom BG, DeSimone DW. Active zones on motor nerve terminals contain alpha 3beta 1 integrin. J Neurosci 2000;20:4912–4921. [PubMed: 10864949]

Daggett DF, Cohen MW, Stone D, Nikolics K, Rauvala H, Peng HB. The role of an agrin-growth factor interaction in ACh receptor clustering. Mol Cell Neurosci 1996;8:272–285. [PubMed: 9026315]

Daniels RW, Gelfand MV, Collins CA, Di-Antonio A. Visualizing glutamatergic cell bodies and synapses in Drosophila larval and adult CNS. J Comp Neurol 2008;508:131–152. [PubMed: 18302156]

DeChiara TM, Bowen DC, Valenzuela DM, Simmons MV, Poueymirou WT, Thomas S, Kinetz E, Compton DL, Rojas E, Park JS, Smith C, DiStefano PS, Glass DJ, Burden SJ, Yancopoulos GD. The receptor tyrosine kinase MuSK is required for neuromuscular junction formation in vivo. Cell 1996;85:501–512. [PubMed: 8653786]

Etzler ME, Kabat EA. Purification and characterization of a lectin (plant hemagglutinin) with blood group A specificity from Dolichos biflorus. Biochemistry 1970;9:869–877. [PubMed: 4984730]

Featherstone DE, Rushton EM, Hilderbrand-Chae M, Phillips AM, Jackson FR, Broadie K. Presynaptic glutamic acid decarboxylase is required for induction of the postsynaptic receptor field at a glutamatergic synapse. Neuron 2000;27:71–84. [PubMed: 10939332]

Featherstone DE, Rushton E, Broadie K. Developmental regulation of glutamate receptor field size by nonvesicular glutamate release. Nat Neurosci 2002;5:141–146. [PubMed: 11753421]

Fyrberg C, Becker J, Barthmaier P, Mahaffey J, Fyrberg E. A Drosophila muscle-specific gene related to the mouse quaking locus. Gene 1997;197:315–323. [PubMed: 9332381]

Gautam M, Noakes PG, Mudd J, Nichol M, Chu GC, Sanes JR, Merlie JP. Failure of postsynaptic specialization to develop at neuromuscular junctions of rapsyn-deficient mice. Nature 1995;377:232–236. [PubMed: 7675108]

Gautam M, Noakes PG, Moscoso L, Rupp F, Scheller RH, Merlie JP, Sanes JR. Defective neuromuscular synaptogenesis in agrin-deficient mutant mice. Cell 1996;85:525–535. [PubMed: 8653788]

Grotewiel MS, Beck CD, Wu KH, Zhu XR, Davis RL. Integrin-mediated short-term memory in Drosophila. Nature 1998;391:455–460. [PubMed: 9461212]

Hacker U, Nybakken K, Perrimon N. Heparan sulphate proteoglycans: the sweet side of development. Nat Rev Mol Cell Biol 2005;6:530–541. [PubMed: 16072037]

Haines N, Seabrooke S, Stewart BA. Dystroglycan and protein O-mannosyl-transferases 1 and 2 are required to maintain integrity of Drosophila larval muscles. Mol Biol Cell 2007;18:4721–4730. [PubMed: 17881734]

Hartig W, Brauer K, Bigl V, Bruckner G. Chondroitin sulfate proteoglycan-immunoreactivity of lectin-labeled perineuronal nets around parvalbumin-containing neurons. Brain Res 1994;635:307–311. [PubMed: 8173967]

Hynes RO. Integrins: bidirectional, allosteric signaling machines. Cell 2002;110:673–687. [PubMed: 12297042]

Iglesias M, Ribera J, Esquerda JE. Treatment with digestive agents reveals several glycoconjugates specifically associated with rat neuromuscular junction. Histochemistry 1992;97:125–131. [PubMed: 1559843]

Jannuzi AL, Bunch TA, West RF, Brower DL. Identification of integrin beta subunit mutations that alter heterodimer function in situ. Mol Biol Cell 2004;15:3829–3840. [PubMed: 15194810]

Johansen J, Halpern ME, Johansen KM, Keshishian H. Stereotypic morphology of glutamatergic synapses on identified muscle cells of Drosophila larvae. J Neurosci 1989;9:710–725. [PubMed: 2563766]

John N, Krugel H, Frischknecht R, Smalla KH, Schultz C, Kreutz MR, Gundelfinger ED, Seidenbecher CI. Brevican-containing perineuronal nets of extracellular matrix in dissociated hippocampal primary cultures. Mol Cell Neurosci 2006;31:774–784. [PubMed: 16503162]

Johnson KG, Tenney AP, Ghose A, Duckworth AM, Higashi ME, Parfitt K, Marcu O, Heslip TR, Marsh JL, Schwarz TL, Flanagan JG, Van Vactor D. The HSPGs Syndecan and Dallylike bind the receptor phosphatase LAR and exert distinct effects on synaptic development. Neuron 2006;49:517–531. [PubMed: 16476662]

Kawaguchi SY, Hirano T. Integrin alpha3beta1 suppresses long-term potentiation at inhibitory synapses on the cerebellar Purkinje neuron. Mol Cell Neurosci 2006;31:416–426. [PubMed: 16307893]

Koirala S, Qiang H, Ko CP. Reciprocal interactions between perisynaptic Schwann cells and regenerating nerve terminals at the frog neuromuscular junction. J Neurobiol 2000;44:343–360. [PubMed: 10942887]

Kramar EA, Lin B, Rex CS, Gall CM, Lynch G. Integrin-driven actin polymerization consolidates long-term potentiation. Proc Natl Acad Sci USA 2006;103:5579–5584. [PubMed: 16567651]

Kummer TT, Misgeld T, Sanes JR. Assembly of the postsynaptic membrane at the neuromuscular junction: paradigm lost. Curr Opin Neurobiol 2006;16:74–82. [PubMed: 16386415]

Landgraf M, Sanchez-Soriano N, Technau GM, Urban J, Prokop A. Charting the Drosophila neuropile: a strategy for the standardised characterisation of genetically amenable neurites. Dev Biol 2003;260:207–225. [PubMed: 12885565]

Leptin M, Bogaert T, Lehmann R, Wilcox M. The function of PS integrins during Drosophila embryogenesis. Cell 1989;56:401–408. [PubMed: 2492451]

Lin B, Arai AC, Lynch G, Gall CM. Integrins regulate NMDA receptor-mediated synaptic currents. J Neurophysiol 2003;89:2874–2878. [PubMed: 12740418]

Lin DM, Goodman CS. Ectopic and increased expression of Fasciclin II alters motoneuron growth cone guidance. Neuron 1994;13:507–523. [PubMed: 7917288]

Lin W, Burgess RW, Dominguez B, Pfaff SL, Sanes JR, Lee KF. Distinct roles of nerve and muscle in postsynaptic differentiation of the neuromuscular synapse. Nature 2001;410:1057–1064. [PubMed: 11323662]

Marangi PA, Wieland ST, Fuhrer C. Laminin-1 redistributes postsynaptic proteins and requires rapsyn, tyrosine phosphorylation, and Src and Fyn to stably cluster acetylcholine receptors. J Cell Biol 2002;157:883–895. [PubMed: 12034776]

Martin PT. Glycobiology of the neuromuscular junction. J Neurocytol 2003;32:915–929. [PubMed: 15034276]

Martin PT, Sanes JR. Role for a synapse-specific carbohydrate in agrin-induced clustering of acetylcholine receptors. Neuron 1995;14:743–754. [PubMed: 7718237]

Mathew D, Ataman B, Chen J, Zhang Y, Cumberledge S, Budnik V. Wingless signaling at synapses is through cleavage and nuclear import of receptor DFrizzled2. Science 2005;310:1344–1347. [PubMed: 16311339]

Misgeld T, Kummer TT, Lichtman JW, Sanes JR. Agrin promotes synaptic differentiation by counteracting an inhibitory effect of neurotransmitter. Proc Natl Acad Sci USA 2005;102:11088–11093. [PubMed: 16043708]

Moransard M, Borges LS, Willmann R, Marangi PA, Brenner HR, Ferns MJ, Fuhrer C. Agrin regulates rapsyn interaction with surface acetylcholine receptors, and this underlies cytoskeletal anchoring and clustering. J Biol Chem 2003;278:7350–7359. [PubMed: 12486121]

Packard M, Koo ES, Gorczyca M, Sharpe J, Cumberledge S, Budnik V. The Drosophila Wnt, wingless, provides an essential signal for pre- and postsynaptic differentiation. Cell 2002;111:319–330. [PubMed: 12419243]

Parkhomovskiy N, Martin PT. Alpha-galactosidase stimulates acetylcholine receptor aggregation in skeletal muscle cells via PNA-binding carbohydrates. Biochem Biophys Res Commun 2000;270:899–902. [PubMed: 10772922]

Parnas D, Haghighi AP, Fetter RD, Kim SW, Goodman CS. Regulation of postsynaptic structure and protein localization by the Rho-type guanine nucleotide exchange factor dPix. Neuron 2001;32:415–424. [PubMed: 11709153]

Pavlov I, Lauri S, Taira T, Rauvala H. The role of ECM molecules in activity-dependent synaptic development and plasticity. Birth Defects Res C Embryo Today 2004;72:12–24. [PubMed: 15054901]

Peng HB, Baker LP, Chen Q. Induction of synaptic development in cultured muscle cells by basic fibroblast growth factor. Neuron 1991;6:237–246. [PubMed: 1847064]

Peng HB, Ali AA, Dai Z, Daggett DF, Raulo E, Rauvala H. The role of heparin-binding growth-associated molecule (HB-GAM) in the postsynaptic induction in cultured muscle cells. J Neurosci 1995;15:3027–3038. [PubMed: 7722643]

Prokop A. Integrating bits and pieces: synapse structure and formation in Drosophila embryos. Cell Tissue Res 1999;297:169–186. [PubMed: 10470487]

Prokop A, Martin-Bermudo MD, Bate M, Brown NH. Absence of PS integrins or laminin A affects extracellular adhesion, but not intracellular assembly, of hemiadherens and neuromuscular junctions in Drosophila embryos. Dev Biol 1998;196:58–76. [PubMed: 9527881]

Puri KD, Gopalakrishnan B, Surolia A. Carbohydrate binding specificity of the Tn-antigen binding lectin from Vicia villosa seeds (VVLB4). FEBS Lett 1992;312:208–212. [PubMed: 1426254]

Qin G, Schwarz T, Kittel RJ, Schmid A, Rasse TM, Kappei D, Ponimaskin E, Heckmann M, Sigrist SJ. Four different subunits are essential for expressing the synaptic glutamate receptor at neuromuscular junctions of Drosophila. J Neurosci 2005;25:3209–3218. [PubMed: 15788778]

Ribera J, Esquerda JE, Comella JX. Phylogenetic polymorphism on lectin binding to junctional and non-junctional basal lamina at the vertebrate neuromuscular junction. Histochemistry 1987;87:301–307. [PubMed: 3121544]

Rohrbough J, Broadie K. Electrophysiological analysis of synaptic transmission in central neurons of Drosophila larvae. J Neurophysiol 2002;88:847–860. [PubMed: 12163536]

Rohrbough J, Grotewiel MS, Davis RL, Broadie K. Integrin-mediated regulation of synaptic morphology, transmission, and plasticity. J Neurosci 2000;20:6868–6878. [PubMed: 10995831]

Rohrbough J, Rushton E, Palanker L, Woodruff E, Matthies HJ, Acharya U, Acharya JK, Broadie K. Ceramidase regulates synaptic vesicle exocytosis and trafficking. J Neurosci 2004;24:7789–7803. [PubMed: 15356190]

Rohrbough J, Rushton E, Woodruff E 3rd, Fergestad T, Vigneswaran K, Broadie K. Presynaptic establishment of the synaptic cleft extracellular matrix is required for post-synaptic differentiation. Genes Dev 2007;21:2607–2628. [PubMed: 17901219]

Rooney JE, Welser JV, Dechert MA, Flintoff-Dye NL, Kaufman SJ, Burkin DJ. Severe muscular dystrophy in mice that lack dystrophin and alpha7 integrin. J Cell Sci 2006;119:2185–2195. [PubMed: 16684813]

Saito S, Nii Y, Taniguchi K. Heterogeneous expression of glycoconjugates among individual glomeruli of the hamster main olfactory bulb. Chem Senses 1999;24:509–515. [PubMed: 10576258]

Sanes JR, Cheney JM. Lectin binding reveals a synapse-specific carbohydrate in skeletal muscle. Nature 1982;300:646–647. [PubMed: 7144916]

Schwander M, Shirasaki R, Pfaff SL, Muller U. Beta1 integrins in muscle, but not in motor neurons, are required for skeletal muscle innervation. J Neurosci 2004;24:8181–8191. [PubMed: 15371519]

Schwarzbauer JE, Sechler JL. Fibronectin fibrillogenesis: a paradigm for extracellular matrix assembly. Curr Opin Cell Biol 1999;11:622–627. [PubMed: 10508649]

Scott LJ, Bacou F, Sanes JR. A synapse-specific carbohydrate at the neuromuscular junction: association with both acetylcholinesterase and a glycolipid. J Neurosci 1988;8:932–944. [PubMed: 3346730]

Shi Y, Ethell IM. Integrins control dendritic spine plasticity in hippocampal neurons through NMDA receptor and Ca2+/calmodulin-dependent protein kinase II-mediated actin reorganization. J Neurosci 2006;26:1813–1822. [PubMed: 16467530]

St John JA, Key B. Heterogeneity in olfactory neurons in mouse revealed by differential expression of glycoconjugates. Histochem J 2002;34:281–289. [PubMed: 12769259]

Staubli U, Chun D, Lynch G. Time-dependent reversal of long-term potentiation by an integrin antagonist. J Neurosci 1998;18:3460–3469. [PubMed: 9547253]

Stewart BA, Schuster CM, Goodman CS, Atwood HL. Homeostasis of synaptic transmission in Drosophila with genetically altered nerve terminal morphology. J Neurosci 1996;16:3877–3886. [PubMed: 8656281]

Suzuki K, Grinnell AD, Kidokoro Y. Hypertonicity-induced transmitter release at Drosophila neuromuscular junctions is partly mediated by integrins and cAMP/protein kinase A. J Physiol 2002;538:103–119. [PubMed: 11773320]

Tisay KT, St John JA, Key B. Expression of specific glycoconjugates in both primary and secondary olfactory pathways in BALB/C mice. J Comp Neurol 2002;443:213–225. [PubMed: 11807832]

Tojo SJ, Germeraad S, King DS, Fristrom JW. Polarized secretion of an ectopic protein in Drosophila salivary glands in vivo. Embo J 1987;6:2249–2254. [PubMed: 3117529]

van der Flier A, Sonnenberg A. Function and interactions of integrins. Cell Tissue Res 2001;305:285–298. [PubMed: 11572082]

van der Plas MC, Pilgram GS, Plomp JJ, de Jong A, Fradkin LG, Noordermeer JN. Dystrophin is required for appropriate retrograde control of neurotransmitter release at the Drosophila neuromuscular junction. J Neurosci 2006;26:333–344. [PubMed: 16399704]

Van Vactor D, Wall DP, Johnson KG. Heparan sulfate proteoglycans and the emergence of neuronal connectivity. Curr Opin Neurobiol 2006;16:40–51. [PubMed: 16417999]

Vogel Z, Christian CN, Vigny M, Bauer HC, Sonderegger P, Daniels MP. Laminin induces acetylcholine receptor aggregation on cultured myotubes and enhances the receptor aggregation activity of a neuronal factor. J Neurosci 1983;3:1058–1068. [PubMed: 6341513]

Wagh DA, Rasse TM, Asan E, Hofbauer A, Schwenkert I, Durrbeck H, Buchner S, Dabauvalle MC, Schmidt M, Qin G, Wichmann C, Kittel R, Sigrist SJ, Buchner E. Bruchpilot, a protein with homology to ELKS/CAST, is required for structural integrity and function of synaptic active zones in Drosophila. Neuron 2006;49:833–844. [PubMed: 16543132]

Wairkar YP, Fradkin LG, Noordermeer JN, DiAntonio A. Synaptic defects in a Drosophila model of congenital muscular dystrophy. J Neurosci 2008;28:3781–3789. [PubMed: 18385336]

Walsh EP, Brown NH. A screen to identify Drosophila genes required for integrin-mediated adhesion. Genetics 1998;150:791–805. [PubMed: 9755209]

Watty A, Burden SJ. MuSK glycosylation restrains MuSK activation and acetylcholine receptor clustering. J Biol Chem 2002;277:50457–50462. [PubMed: 12399462]

Weston CA, Teressa G, Weeks BS, Prives J. Agrin and laminin induce acetylcholine receptor clustering by convergent, Rho GTPase-dependent signaling pathways. J Cell Sci 2007;120:868–875. [PubMed: 17298982]

Whitelock JM, Iozzo RV. Heparan sulfate: a complex polymer charged with biological activity. Chem Rev 2005;105:2745–2764. [PubMed: 16011323]

Zhou H, Muramatsu T, Halfter W, Tsim KW, Peng HB. A role of midkine in the development of the neuromuscular junction. Mol Cell Neurosci 1997;10:56–70. [PubMed: 9361288]

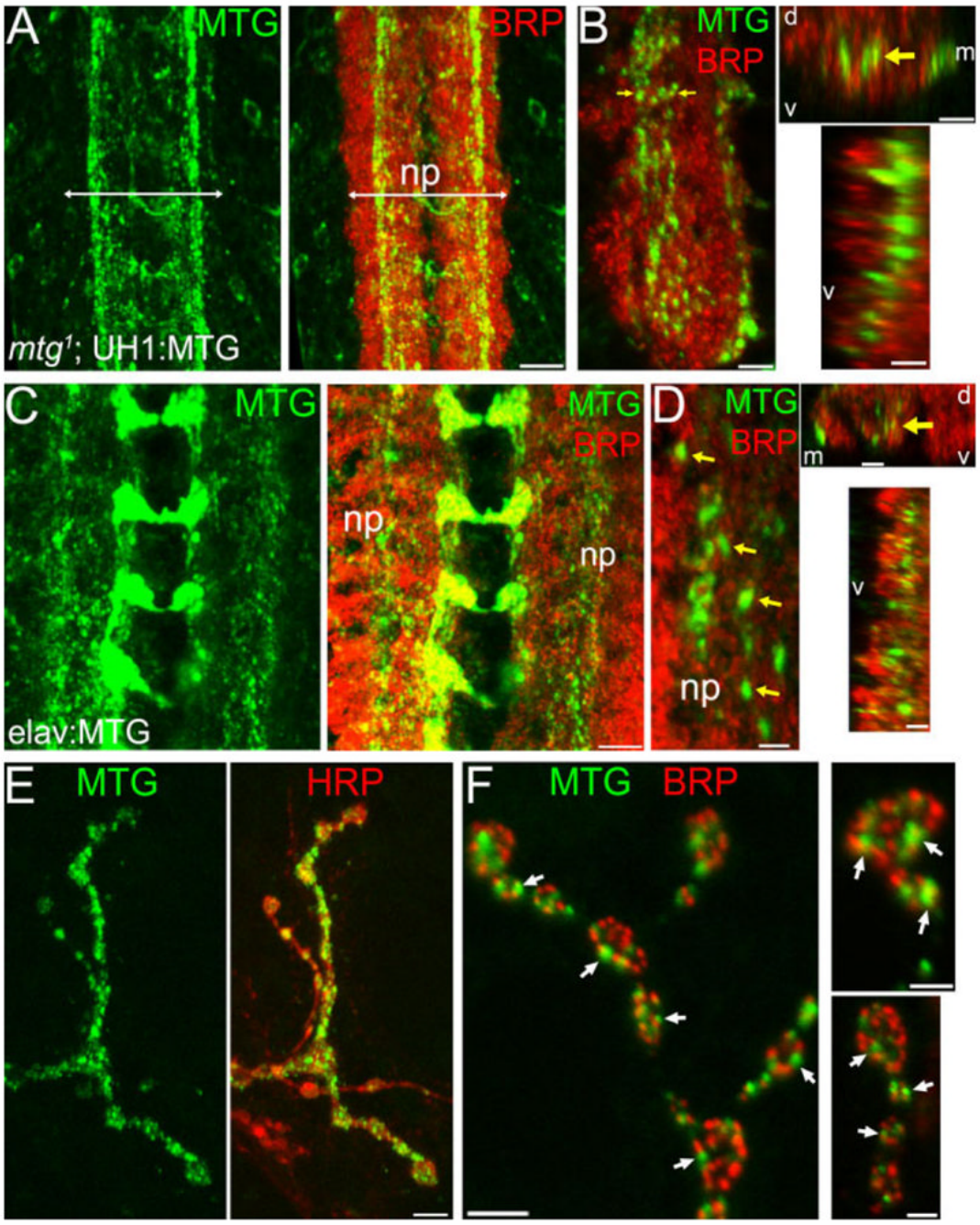

Fig. 1.

MTG is synaptically localized in both CNS and neuromuscular junction. A,B: *mtg*^{1} larva rescued by UH1-driven UAS-MTG::GFP (*mtg*^{1}; UH1:MTG) shortly after hatching. Anti-GFP (green); anti-BRP (red). **A:** MTG::GFP aggregates in longitudinal and transverse processes within neuropil (np; arrows indicate lateral np boundaries); 15-μm Z-stacks. **B:** Left: Higher magnification of MTG::GFP puncta; 3 posterior neuronal hemisegments are shown (5-μm Z-stack). Top right: Transverse cross-section through the neuropil; yellow arrows show the same position in both orientations. Bottom right: Longitudinal cross-section through the CNS neuropil. d, dorsal; v, ventral; m, medial). C,D: *elav*:MTG in mature larvae. **C:** MTG::GFP (green) predominantly restricted to synaptic neuropil, labeled with BRP (red) (10-μm Z-stack).

Note MTG::GFP in horizontal commissures. **D:** Left: Higher magnification of MTG puncta (yellow arrows) within neuropil (5-μm Z-stack). Right: Transverse (top) and longitudinal cross-sections (bottom) through the neuropil as in B. Preparations A–D were detergent-treated. E,F: MTG::GFP expression at NMJ. **E:** Muscle 12 NMJ in *elav*:MTG larva. Native MTG::GFP fluorescence (green, left); anti-HRP (red, right); detergent-free. **F:** Anti-GFP and anti-BRP co-labeled NMJs (detergent-treated) showing MTG punctae (arrows) localized adjacent to BRP punctae. Right: Higher-magnification of boutons. Scale bars = 10 μm (A, C); 4 μm (B; D, left); 5 μm (D, right; E); 2 μm (F, left); 1 μm (F, right).

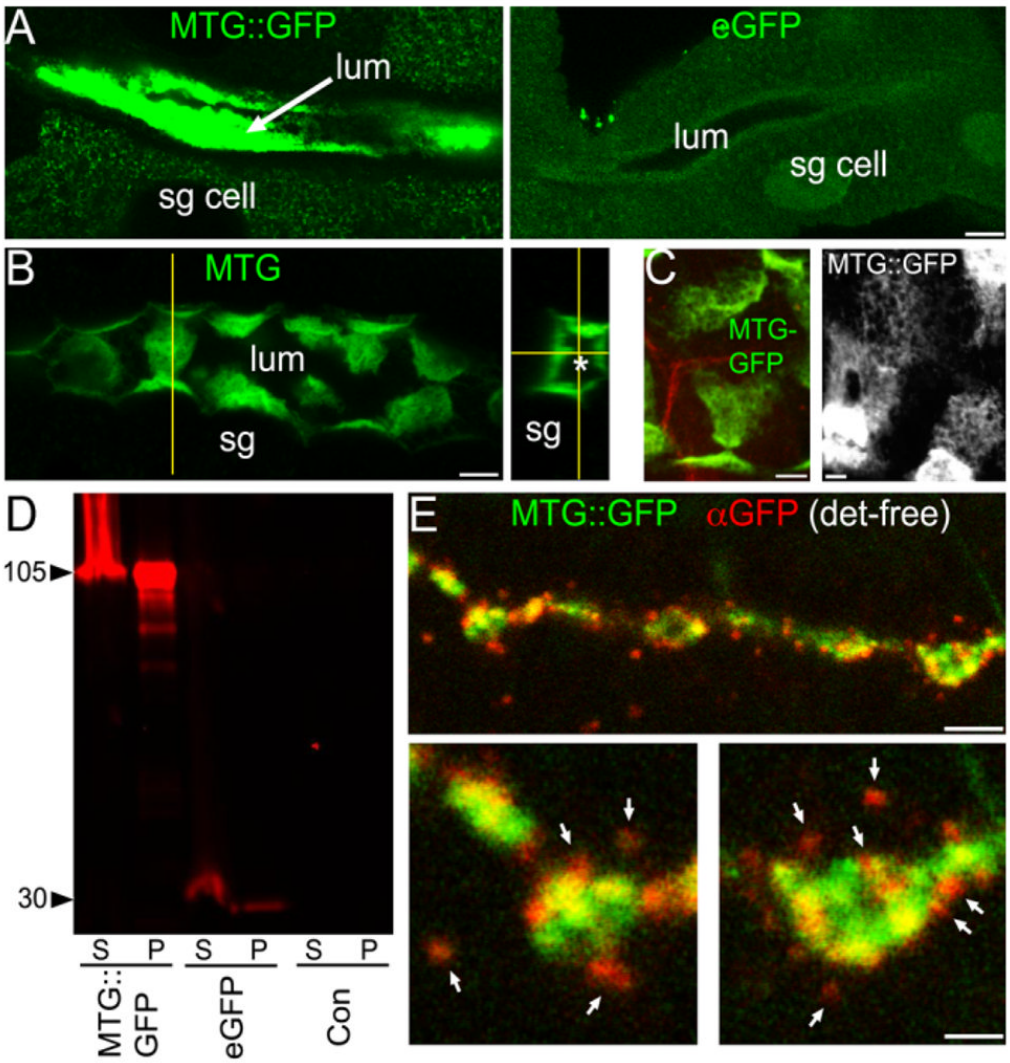

Fig. 2.

MTG is secreted and associates closely with the cell surface. **A:** Left: *elav*:MTG in the salivary gland (SG) lumen (large arrow). Right: *elav*:eGFP within SG cytoplasm and nuclei. **B:** Extracellular MTG::GFP in the SG (anti-GFP). Left: 5-μm Z-stack, showing lumenal surface of SG cells. Vertical yellow line marks the point of a confocally reconstructed cross-section (right); asterisk (*) marks center of lumen. **C:** High-magnification thin sections showing MTG::GFP associated with secretory cell membranes, and revealing outlines of fused vesicles. Left: anti-GFP (green); anti-HRP (red) reveals SG membranes. Right: Native MTG::GFP fluorescence coating SG membrane surface. **D:** Western blot of protein extract probed with anti-GFP. S, supernatant; P, pellet. **E:** Briefly-fixed larval NMJ. Native MTG::GFP fluorescence (green); anti-GFP (red), detergent-free. Bottom: Higher-magnification of single boutons. Scale bars = 10 μm (A,B); 4 μm (C); 5 μm (E, top); 2 μm (E, bottom).

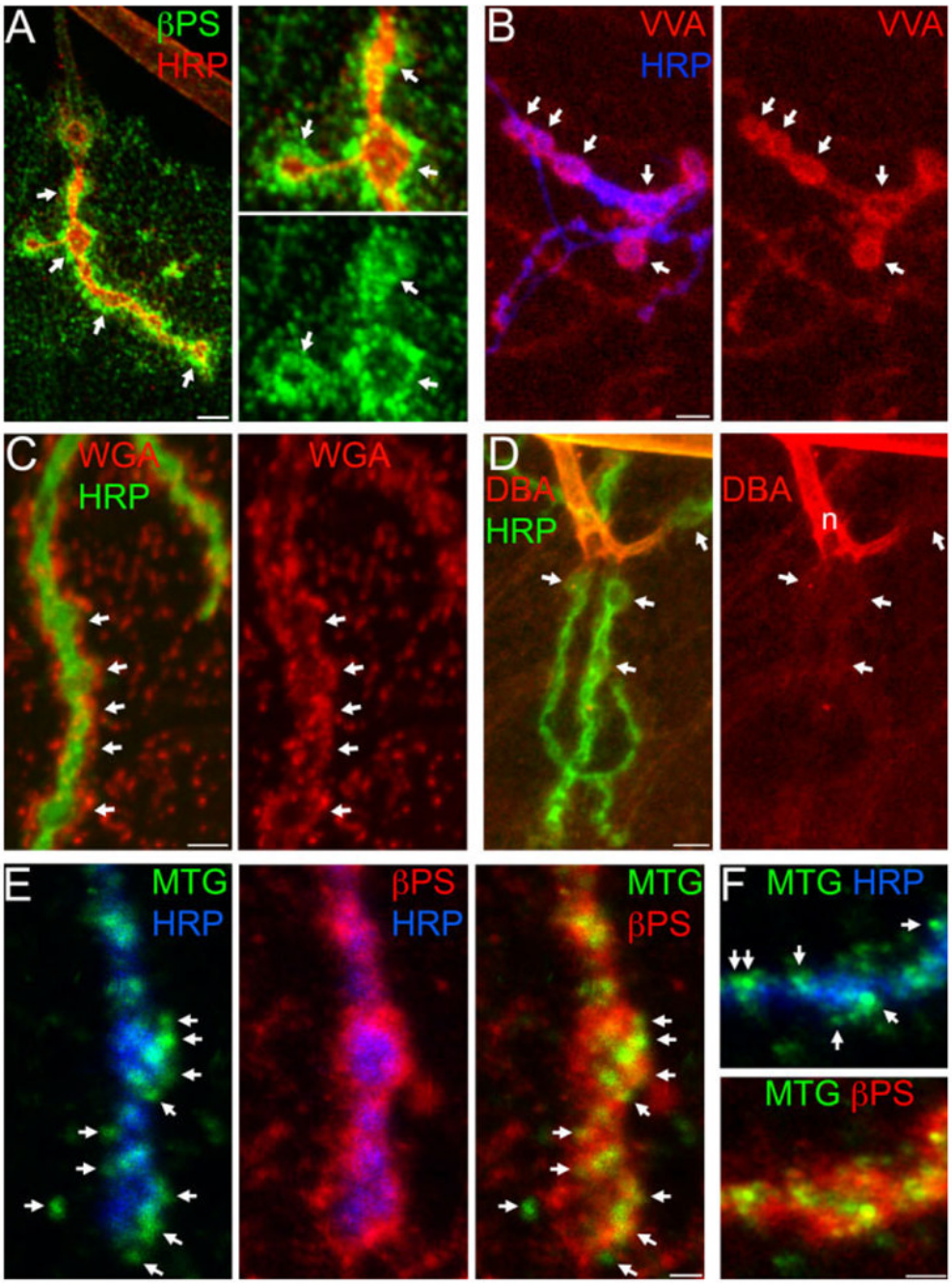

Fig. 3.

Secreted MTG resides within the synaptic matrix environment. A–D: Wandering third instar NMJs probed with integrin antibodies and lectins in detergent-free conditions. **A:** βPS integrin (green); HRP (red). Right: Two-fold increased magnification. Arrows indicate boutons. **B:** TRITC-conjugated VVA lectin (GalNAc-specific; red) and anti-HRP (blue). Arrows indicate type I boutons (NMJ 13). **C:** TRITC-conjugated WGA lectin (GlcNAc-specific, red) and anti-HRP (green). Arrows indicate synaptic boutons. **D:** TRITC-conjugated DBA (GalNAc-specific; red) and HRP (green). Arrows indicate synaptic boutons. E,F: Anti-GFP (green) staining for MTG::GFP, colocalized with anti-βPS in elav:MTG::GFP larvae (detergent-free conditions). E–F: *elav*:MTG NMJs. **E:** Left: anti-GFP puncta (green) and HRP (blue); middle:

βPS (red) and HRP; right: anti-GFP colocalized with βPS. Arrows indicate clear extracellular anti-GFP punctae. **F:** Anti-GFP punctae (green) at NMJs boutons costained with HRP (blue, top panel) contained within the βPS integrin domain (red; bottoms panel). Arrows (top) indicate extracellular MTG::GFP punctae. Scale bars = 5 μm (A, left; B–D); 2.5 μm (A, right); 2.5 μm (E,F).

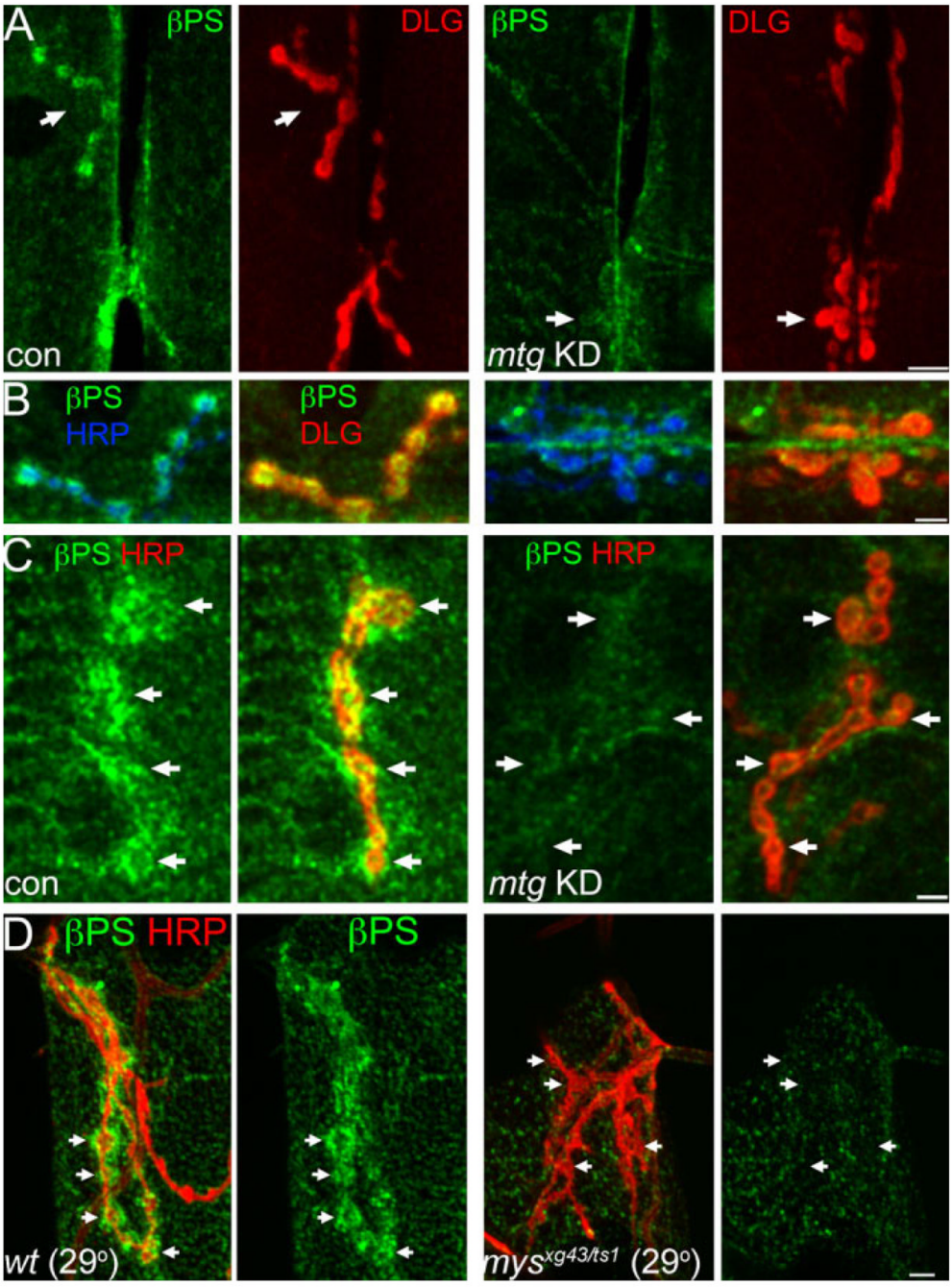

Fig. 4.

Presynaptic MTG regulates postsynaptic integrin receptor expression. A–C: Synaptic βPS integrin levels are reduced by presynaptically targeted *mtg* RNAi. **A:** Anti-βPS (green) and anti-DLG (red) in *elav*-GAL4/+ control (con) and presynaptic *mtg* KD RNAi (*elav*-GAL4/+; UAS-*mtg* RNAi/*mtg*^{1}). NMJ 6/7 shown for both genotypes. **B:** Magnified NMJ subregions indicated by arrows in A for control (left) and *elav:mtg*RNAi (right). Left: βPS (green) surrounding HRP-stained presynaptic boutons (blue). Right: Largely overlapping βPS and DLG domains. **C:** Higher-magnification images showing reduction of synaptic βPS (green) in presynaptic *mtg* KD larvae (right). Arrows indicate individual boutons. Co-stained with anti-HRP (red). **D:** Comparative loss of synaptic βPS expression (green) in *mys*^{ts1}/*mys*^{xg43}. Mutants

raised at 29°C (right); wildtype control (left), muscle 12 NMJ costained with anti-HRP (red). Arrows indicate individual synaptic boutons. Detergent-free. Scale bars = 10 μm (A); 5 μm (B–D).

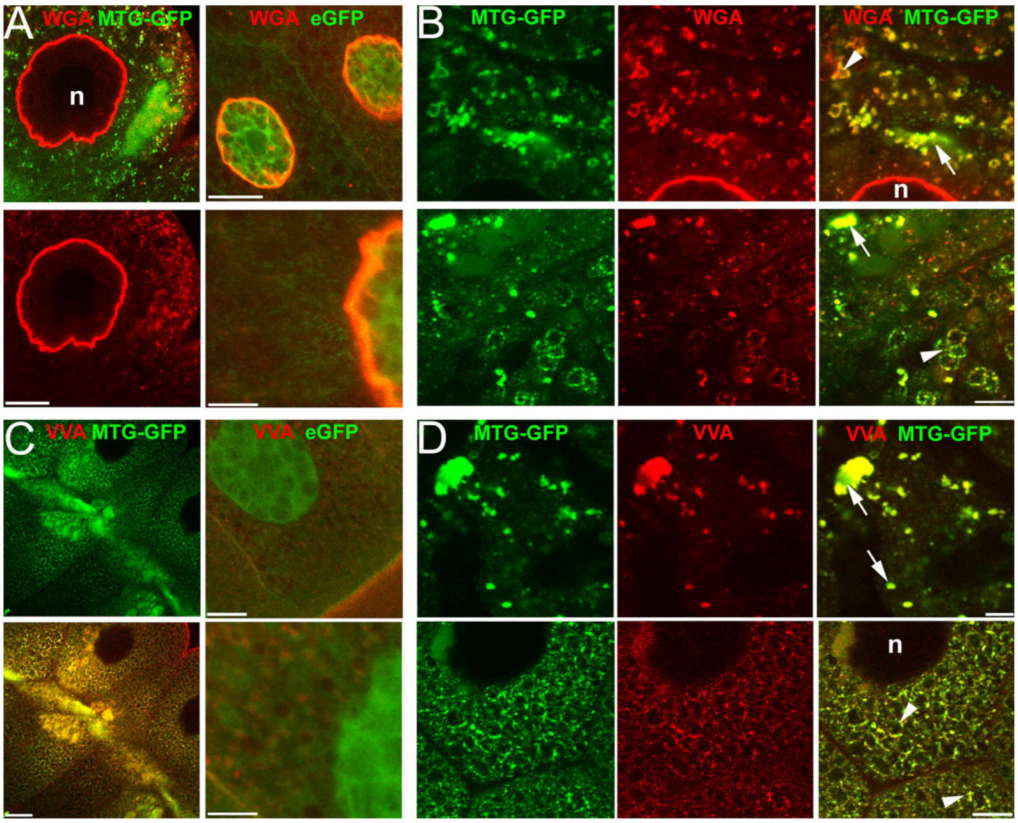

Fig. 5.

MTG regulates the carbohydrate environment in the salivary gland. GFP native fluorescence (green) and lectin labeling (red) in detergent-treated salivary glands (SG) expressing MTG::GFP or eGFP. A,B: SG cells stained with WGA. **A:** Left: MTG::GFP and WGA co-localized in the secretory pathway in the cytoplasm. Right: eGFP control at low (top) and high magnification (bottom). **B:** Examples of MTG::GFP/WGA co-localization. Arrows indicate large and small accumulations; arrowheads indicate secretory vesicles. C,D: SG cells stained with VVA. **C:** Left: MTG::GFP accumulated and co-localized with VVA in the cytoplasm. Right: eGFP control at low (top) and high magnification (bottom). **D:** Examples of MTG::GFP/VVA co-localization. Arrows indicate large and small accumulations; arrowheads indicate secretory vesicles. Scale bars = 10 μm (A, left); 20 μm (A, right, top); 5 μm (A, right, bottom); 10 μm (B); 20 μm (C, left); 10 μm (C, right, top); 5 μm (C, right, bottom); 10 μm (D). n, nucleus.

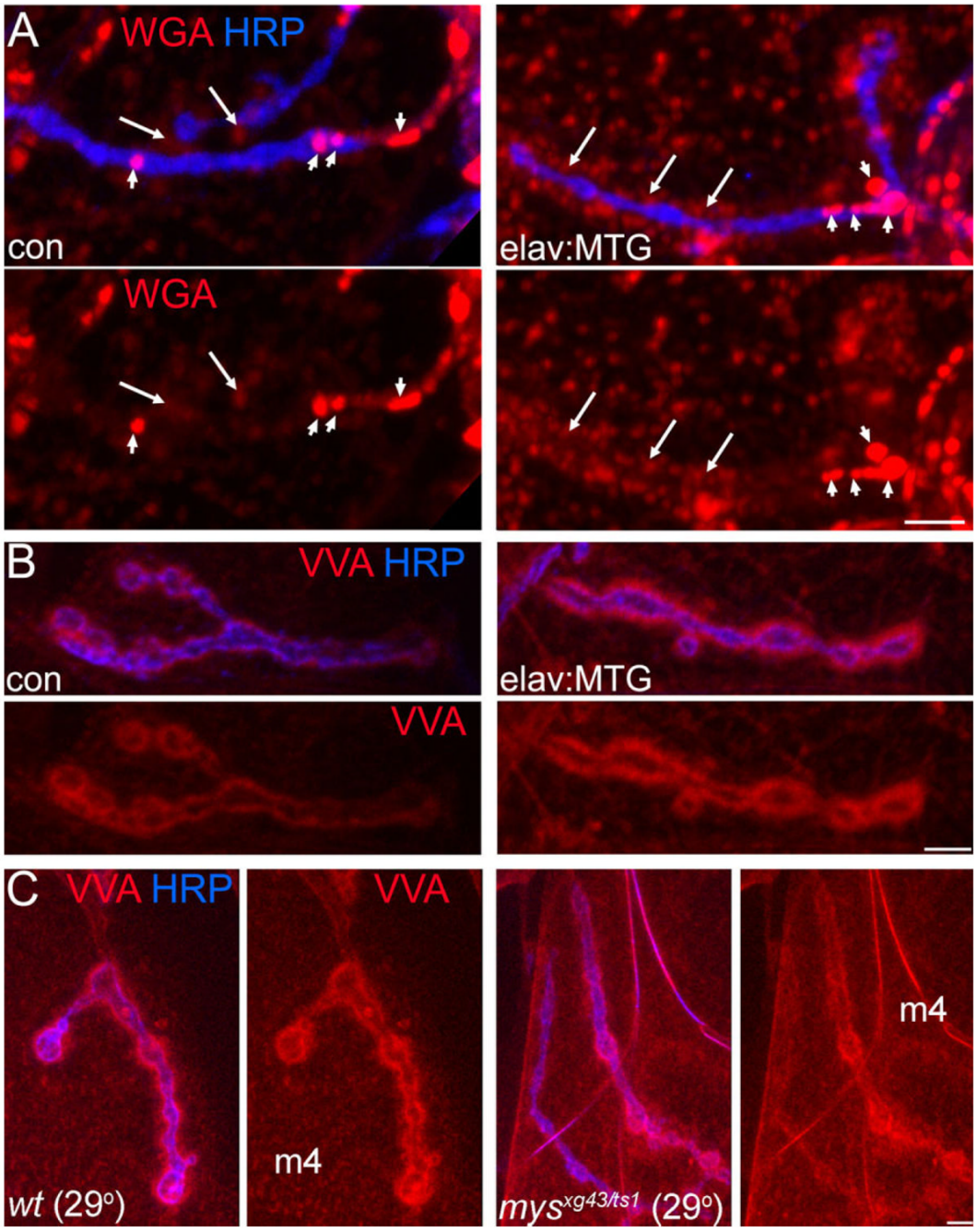

Fig. 6.

Presynaptic MTG regulates the synaptic ECM carbohydrate matrix. **A:** WGA-binding carbohydrates at the NMJ are upregulated by targeted neuronal MTG overexpression. Third instar NMJs from *elav*-GAL4/+ control (con; left) and *elav*:MTG (right) probed with TRITC-WGA (red) and anti-HRP (blue). Short arrows point to saturated WGA puncta; long arrows point to diffuse WGA outlining NMJ. **B:** VVA-binding carbohydrates are upregulated by neuronal MTG overexpression. Similar preparations as for WGA, but stained with TRITC-VVA. **C:** Integrins regulate the synaptic selectivity of VVA-labeled ECM carbohydrates. VVA (red) and anti-HRP labeling (blue) in control (left) and mys^{ts1}/mys^{xg43} mutant NMJs (right),

showing elevated nonsynaptic expression in the mutant muscle. All panels show muscle 4 NMJ; detergent-free conditions were used for all results shown. Scale bars = 5 μm.

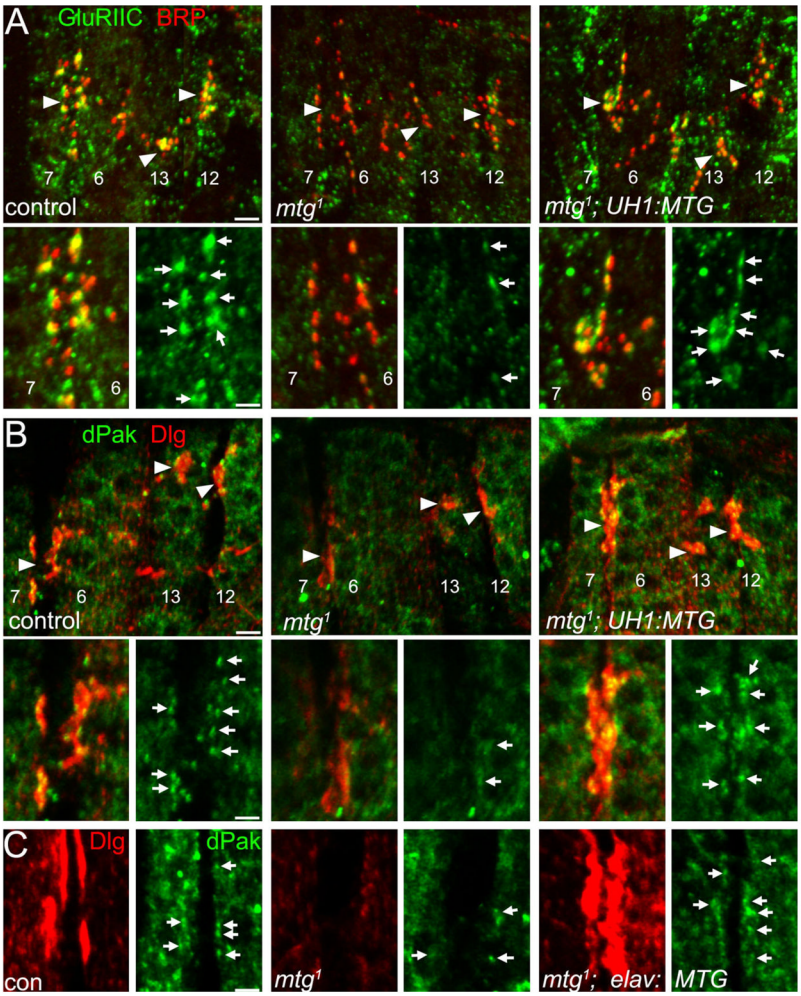

Fig. 7.

Transgenic MTG rescue of postsynaptic assembly in *mtg* null mutant. **A:** Postsynaptic GluRIIC (green) and presynaptic BRP (red) immunostaining in mtg^{+} control (UAS-MTG::GFP/+; left panels), *mtg*^{1} null mutant *(*UAS-MTG::GFP/+; *mtg*^{1}; center panels), and *mtg*^{1} null mutant rescued by UH1-driven UAS-MTG::GFP (*mtg*^{1}; UH1:MTG; right panels). Top: Merged GluRIIC and BRP localization at NMJs 6/7, 13, and 12 (arrowheads). Bottom: Muscle 6/7 NMJ in greater detail. **B:** Postsynaptic DLG (red) and dPak (green) immunostaining in mtg^{+} control (left), *mtg*^{1} null mutant (center), and *mtg*^{1}; UH1:MTG rescued embryo (right). Top: Merged DLG and dPak localization at NMJs 6/7, 13, and 12 (arrowheads). Bottom: Muscle 6/7 NMJs in greater detail. **C:** Synaptic rescue in *mtg*^{1} null mutants by neuronally-targeted *elav*-driven MTG::GFP (*mtg*^{1}; elav:MTG). Postsynaptic DLG (red; left) and dPak (green; right) immunostaining at the muscle 6/7 NMJ in mtg^{+} control (left), *mtg*^{1} null mutant (center), and *mtg*^{1}; *elav*:MTG rescued embryo (right). Scale bars = 5 μm (A,B, top), 2 μm (A,B, bottom; and C).